Quaternary Science Reviews 297 (2022) 107788

Contents lists available at ScienceDirect

Quaternary Science Reviews

journal homepage: www.elsevier.com/locate/quascirev

Towards an astronomical age model for the Lower to Middle Pleistocene hominin-bearing succession of the Sangiran Dome area on Java, Indonesia

Sander L. Hilgen [a, b, *], Frederik J. Hilgen [c], Shinatria Adhityatama [d], Klaudia F. Kuiper [b], Josephine C.A. Joordens [a, b, e, f]

[a] Naturalis Biodiversity Center, P.O. Box 9517, Leiden, the Netherlands
[b] Faculty of Science, Vrije Universiteit, de Boelelaan 1085, 1081HV, Amsterdam, the Netherlands
[c] Universiteit Utrecht, Heidelberglaan 8, 3584 CS, Utrecht, the Netherlands
[d] Griffith Centre for Social and Cultural Research, Griffith University, Gold Coast, Queensland, Australia
[e] Faculty of Science and Engineering, Maastricht University, Paul-Henri Spaaklaan 1, 6229 EN, Maastricht, the Netherlands
[f] Faculty of Archaeology, Leiden University, P.O. Box 9514, Leiden, the Netherlands

ARTICLE INFO

Article history:
Received 11 March 2022
Received in revised form
23 September 2022
Accepted 23 September 2022
Available online 2 November 2022

Handling Editor: Mira Matthews

Keywords:
Cyclostratigraphy
Middle Pleistocene transition (MPT)
Homo erectus
Sea level changes
Obliquity
Astronomical tuning
Southeastern Asia
Paleoclimatology
Sedimentology
Lakes
Lagoons & swamps

ABSTRACT

Well-dated paleoanthropological sites are critical for studying hominin evolution and dispersal, especially when related to regional or global climate change. For the rich hominin fossil record of Africa, this has been facilitated by the development of high-resolution astronomically tuned age models. So far, such age models are lacking for the Pleistocene of SE Asia with its similarly rich fossil hominin record. This study aims to develop an astronomical age model for the classical Sangiran Dome area of central Java, using a semi-quantitative grain size record of the hominin-bearing Sangiran and Bapang Formations. Two initial age models were established based on two different sets of tie points and approaches (constant sedimentation rate and Bayesian age modelling). These models, which correspond to the paleoanthropological short and long chronologies for the arrival of *Homo erectus* on Java, were used to convert the grain size record into a time series for time series analysis. The preferred initial age model was then used as a starting point to correlate or tune the grain size record to the LR04 benthic $\delta^{18}O$ isotope stack. This tuning was constrained by the sudden switch in grain size from obliquity to double obliquity related cycles; this switch can be linked to the onset of the Mid-Pleistocene Transition at ~1.2 Ma marked by a similarly abrupt change in ice age history. Two slightly different astronomical age models are presented, while a one cycle hiatus at the base of the Grenzbank cannot be excluded. These age models are in better agreement with the short paleoanthropological chronology, arguing for a late arrival of *H. erectus* on Java. Finally, such astronomical age models, when finalized, will provide the accurate, precise, and high-resolution age control required to gain insight into the influence of both regional and global climate change on the Pleistocene paleoenvironment and potentially the hominin population of Java.

1. Introduction

To understand the potential causal relationship between regional and global climate change and hominin evolution and dispersal, high-resolution astronomically dated chronological frameworks for paleoanthropological sites are required. Such frameworks are also needed to independently test astronomical climate-forcing hypotheses in hominin evolution such as those that have been proposed for the Plio-Pleistocene in eastern Africa with its rich and intensively studied hominin fossil record (e.g., Boës et al., 2019; Joordens et al., 2011). These hypotheses include scenarios concerning the origin of new hominin species (Vrba, 1988), the coincidence of major steps in African hominin evolution and aridity (deMenocal, 1995; 2004), and the stimulation of evolutionary change through extreme wet/dry climate variability (Trauth

* Corresponding author. Naturalis Biodiversity Center, P.O. Box 9517, Leiden, the Netherlands.
E-mail address: sander.hilgen@naturalis.nl (S.L. Hilgen).

https://doi.org/10.1016/j.quascirev.2022.107788

et al., 2007) or prolonged periods of high climate variability (Potts and Faith, 2015). Climate change has also been linked to the dispersal of hominin species. For example, the timing and driving force for modern humans to move out of Africa and their subsequent spread over the Asian subcontinent has been linked to favorable dispersal conditions related to astronomically induced monsoonal variations (e.g., Drake et al., 2011; Timmermann and Friedrich, 2016). As such, integrated, astronomically tuned age models not only provide an accurate, precise, and high-resolution chronological framework, but also the means to explore potential driving mechanisms behind hominin evolution and dispersal. However, the relation between human evolution and climate is not unambiguous and should be considered with caution (see Trauth et al., 2021).

Links between astronomically forced global climate change and the stratigraphic succession have also been suggested for the paleoanthropological record of the Indonesian archipelago and Java in particular. For example, the migration of *Homo erectus* from the SE Asian mainland across the exposed Sunda Shelf is thought to have been only possible during low-sea levels associated with glacial periods (Fig. 1A, Storm, 2001). At Mojokerto, East Java, vegetation change inferred from a pollen record is tentatively linked to specific marine oxygen isotope stages (Morley et al., 2020). Another example is the correlation of the Grenzbank, a key lithostratigraphic marker bed at Sangiran, to low-sea levels associated with MIS 22 by Matsu'ura et al. (2020). These authors tentatively link this change in sedimentary environment to the onset of the Mid-Pleistocene Transition (MPT) and speculate about a potential link between the MPT and the transition from an archaic to a more derived form of *H. erectus* on Java.

So far, the high-resolution chronological framework necessary to test these hypotheses in Indonesia is lacking, mainly because of difficulties encountered in dating the mostly volcaniclastic sediments. This is exemplified by the first occurrence date of *H. erectus* at the base of the Upper Sangiran Fm in the Sangiran Dome area (Brasseur et al., 2015; Matsu'ura et al., 2020). The plethora of published ages for the Sangiran Dome area stratigraphic record can broadly be divided into a paleoanthropological long chronology tied to an early arrival of *H. erectus* (>~1.51 Ma; Larick et al., 2001), and a paleoanthropological short chronology which implies a significantly later arrival (<~1.3 Ma; Matsu'ura et al., 2020). The discussion regarding the two chronologies remains unresolved. Although recently significant progress has been made in accurately and precisely dating of several key paleoanthropological sites such as Ngangdong (Rizal et al., 2020) and Sangiran (Matsu'ura et al., 2020), the age control, and especially its resolution, is insufficient to test the potential influence of global and regional climate change on hominin evolution and dispersal in Pleistocene SE Asia.

This study aims to explore the potential of the Sangiran Dome area for constructing an astronomically tuned age model by applying cyclostratigraphic analysis to a sedimentary log of the Pleistocene Sangiran and Bapang Fms constructed from available publications. The objectives are: 1) to assess whether fine/coarse grain size alternations in the Sangiran and Bapang Fms are cyclical, 2) if so, to determine their duration and potential relation to known cycles of astronomical climate forcing (e.g., precession, obliquity, and eccentricity), 3) to test whether the recorded cycles can be correlated to the global benthic $\delta^{18}O$ curve (LR04 stack; Lisiecki and Raymo, 2005) or to regional climate change, and 4) thereby to provide a testable astrochronological age model for the Sangiran and Bapang Fms.

2. Geological background

The island of Java (Fig. 1A) is characterized by a highly active tectonic and volcanic history resulting from the subduction of the Indo-Australian Plate under the Sunda shelf, a southern extension of the Eurasian Plate. Java emerged between 2.6 and 2.0 Ma, with continuing uplift resulting in more widespread emergence after 2.0 Ma (van Gorsel and Troelstra, 1981; Berghuis et al., 2021). Sediments representing this younger part of the geological history of Java are particularly well exposed in the Sangiran Dome area (Fig. 1B). This area is located between the Merapi volcano to the west and the Lawu volcano to the east and is bordered by the

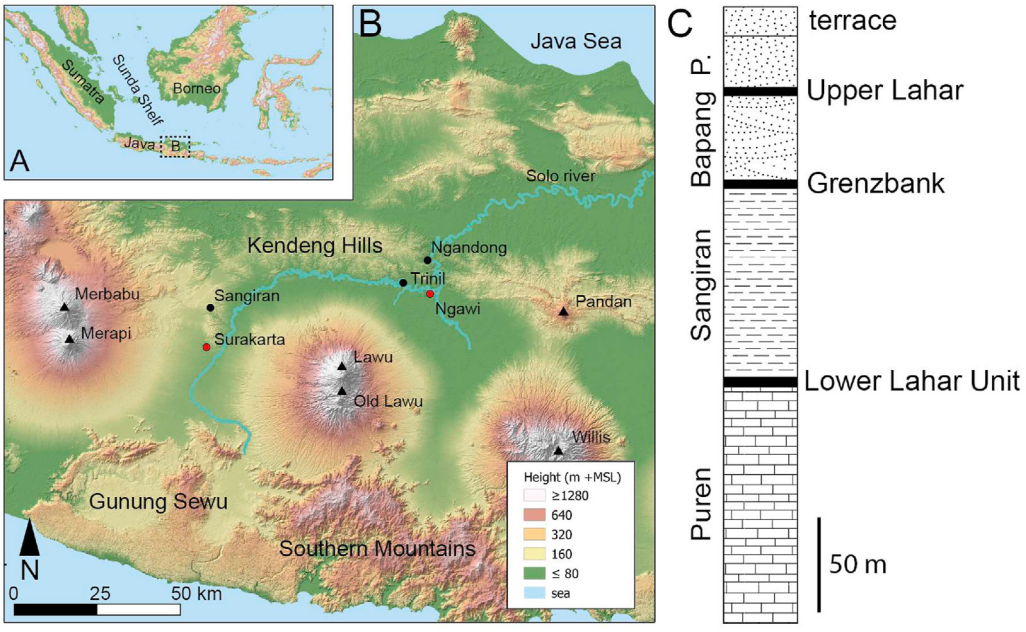

Fig. 1. (a) Overview of the Indonesian archipelago and (b) of central Java. Black triangles indicate volcanoes, red circles indicate larger cities and black circles paleoanthropological sites of interest. (c) Schematic stratigraphic column for the Sangiran Dome area based on Matsu'ura et al. (2020) and references therein. P. = Pohjajar Fm. (For interpretation of the references to colour in this figure legend, the reader is referred to the Web version of this article.)

Kendeng Hills to the north and the Southern Mountains to the south. At the center of the Sangiran Dome area lies a mud volcano that has uplifted the older stratigraphy which was subsequently eroded producing concentric rings with the oldest marine sediments of the Puren Fm exposed in the center and the younger lagoonal and fluviatile sediments of the Sangiran and Bapang Fms exposed towards the outside. For a detailed geological map of the Sangiran Dome area, see Fig. 2 in Itihara et al. (1985b).

The Plio-Pleistocene stratigraphy of the Sangiran Dome area is subdivided into four formations capped by terrace deposits (Fig. 1C; Watanabe and Kadar, 1985; detailed description in Itihara et al., 1985a). At the base of the stratigraphic succession lies the Puren Fm consisting of near-shore marine carbonates and brackish water sediments, followed stratigraphically by the lagoonal and lacustrine Sangiran Fm and the mainly fluviatile sediments of the Bapang Fm. On top of the Bapang Fm lies the Pohjajar Fm, which consists of gravel, sand, silt, and clay of freshwater origin with intercalations of lahars, pumice lenses, and tuff layers. The Sangiran Dome area stratigraphic succession is capped by terrace sediments which can be subdivided into older and younger Terrace deposits (Itihara et al., 1985a). Whereas the exact relation between the older Terrace deposits and the Plio-Pleistocene stratigraphy is unknown, the younger Terrace deposits unconformably overlie the entire Plio-Pleistocene sequence. This study focuses on the Sangiran and Bapang Fms which are presented in more detail below.

2.1. Sangiran Fm

At the base of the Sangiran Fm lies the Lower Lahar Unit (LLU; Fig. 2; Larick et al., 2001). The LLU has a thickness of 0.7–46 m (Itihara et al., 1985a, 1994) and consists of a conglomerate containing andesite fragments, sandstone clasts, clay balls, and pumice in a tuffaceous, medium to coarse sand matrix containing vertebrate fossils, plant remains, mollusk shells, and coral fragments (Bettis et al., 2004). The contact with the underlying Puren Fm is mostly erosive but in some places conformable (Itihara et al., 1985a). Hornblende crystals extracted from detrital pumice derived from the LLU have been $^{40}Ar/^{39}Ar$ dated at 1.90 ± 0.02 Ma (1σ, Bettis III et al., 2004), using a multigrain approach, and at ~1.7 Ma, using a single grain approach. These ages are likely within uncertainty consistent with the inferred presence of the Olduvai subchron within the LLU (Sémah et al., 2000).

On top of the LLU lies the Black Clay of the Sangiran Fm with a total thickness of c. 111.3 m (Fig. 2; Itihara et al., 1985a), ranging from the top of the LLU until the base of the Grenzbank (GB; see section 2.2). Itihara et al. (1985a) subdivide the Black Clay into a lower brackish and marine part and an upper lacustrine part. Alternatively, Brasseur (2009) subdivides the Sangiran Fm into three parts, a Lower, Middle and Upper part (Brasseur, 2009; Brasseur et al., 2015). Although this paper employs the detailed stratigraphy of Itihara et al. (1985a) we adhere to the triple division as defined by Brasseur (2009).

The Lower Sangiran Fm has a thickness of c. 32 m and ranges from the LLU to the base of the diatomite and diatomaceous marls (Fig. 2; Brasseur, 2009). The similarity between the lithological characteristics and the fossil content of the Lower Sangiran Fm and the top of the underlying Puren Fm suggests a continuation of similar environmental conditions (Itihara et al., 1985a). Paleoenvironmental reconstructions show the presence of mangrove forests, coastal swamps, and brackish lakes (A.-M. Sémah, 1982; Brasseur et al., 2015).

The Middle Sangiran Fm has a thickness of c. 44 m and extends from the base of the diatomite and diatomaceous marls to the first septarian carbonate nodule horizon at c. 77.5 m (Fig. 2; Brasseur, 2009). These nodules mark the moment that the Sangiran Dome area becomes dry enough for sufficiently long periods of time to form paleosols. The Middle Sangiran Fm is characterized by widespread, flat marshes that show weak lateral variation (Brasseur et al., 2015). The paleoenvironment of the Middle Sangiran Fm is interpreted as a coastal marsh sedimentary sequence that is episodically connected to a marine environment and occasionally interrupted by ephemeral emersion events (Brasseur et al., 2015). At least two fully marine incursions are present in the Middle Sangiran Fm, indicated by the presence of a c. 2.5 m thick marine diatomite layer at c. 32.7 m and a marine shell bed at c. 37.5 m. Tuff 5, 6, and 8 in the Middle Sangiran Fm have been fission-track dated at, 1.51 ± 0.25 (2σ, Suzuki et al., 1985), 1.49 ± 0.32 (2σ, Suzuki et al., 1985), and 1.345 ± 0.108 Ma (1σ, Matsu'ura et al., 2020), respectively.

The Upper Sangiran Fm has a thickness of c. 35 m and stretches from the first appearance of septarian carbonate nodules until the base of the GB (Fig. 2; Brasseur et al., 2015). Paleosol and palynological studies of the Upper Sangiran Fm indicate alternating drier and wetter environmental conditions (Tokunaga et al., 1985; Brasseur et al., 2015). Drier environmental conditions are suggested by the presence of a semi-arid pedoclimate that is characterized by strong seasonality. During these drier conditions, vegetation consisted of an open savannah cover dominated by grasses and poor in trees and ferns. Wetter episodes are marked by the development of extensive marshes behind mangrove forests with vegetation consisting of grasses, sedges, ferns, reeds, and trees (Tokunaga et al., 1985; Brasseur et al., 2015). The base of the Upper Sangiran Fm is potentially the first appearance date of *H. erectus* at Sangiran (Brasseur et al., 2015; Matsu'ura et al., 2020). Chronological control consists of Tuff 10 at c. 96 m which has been fission-track dated at 1.16 ± 0.24 Ma (2σ, Suzuki et al., 1985). A normal polarity interval has been identified in the Upper Sangiran Fm ranging from just above Tuff 11 to slightly below the base of the GB (Shimizu et al., 1985; Hyodo et al., 1993). This interval is either interpreted as the Jaramillo subchron (0.990–1.070 Ma in GPTS2020, Shimizu et al., 1985; Hyodo et al., 1993) or the Brunhes-Matuyama boundary (0.773 Ma in GPTS2020, F. Sémah, 1982).

2.2. Bapang Fm

At the base of the Bapang Fm lies the conglomeratic Grenzbank (Fig. 2; GB). The GB marks a shift from a relatively low-energy depositional environment to a more high-energy, fluviatile system. This change in the sedimentary environment has been attributed to various phenomena such as volcanic activity (Larick et al., 2001), tectonics (Sémah et al., 2000, 2010), and sea-level change (specifically the GB; Matsu'ura et al., 2020). Although the Bapang Fm shows much more lateral variation than the Sangiran Fm, it consists of semi-regular alternations of gravels and silts in the SE part of the Sangiran Dome area (Larick et al., 2001; Brasseur et al., 2015). These are sometimes referred to as cycles (Bettis et al., 2009), with two distinct sedimentary facies, a lower and coarser a-facies consisting of poorly sorted planar- and cross-bedded gravels and sands, and an upper and finer b-facies consisting of poorly to moderately sorted tuffaceous silts and sands (Larick et al., 2001).

The Bapang Fm contains four important chronologic markers. Firstly, the GB is $^{40}Ar/^{39}Ar$ dated at 1.51 ± 0.08 Ma (2σ) by applying a multigrain approach using hornblende separates from epiclastic pumice (Larick et al., 2001). A significantly younger age of c. 900 ka is proposed for the GB based on fission track and U–Pb ages on pumice and tuff collected from just above the GB and the GB itself (Saleki et al., 1998; Falguères et al., 2016; Matsu'ura et al., 2020). Secondly, the Middle tuff (MT) is dated at 780 ± 150 (2σ, Shimizu et al., 1985). Thirdly, the presence of in-situ Australasian strewn

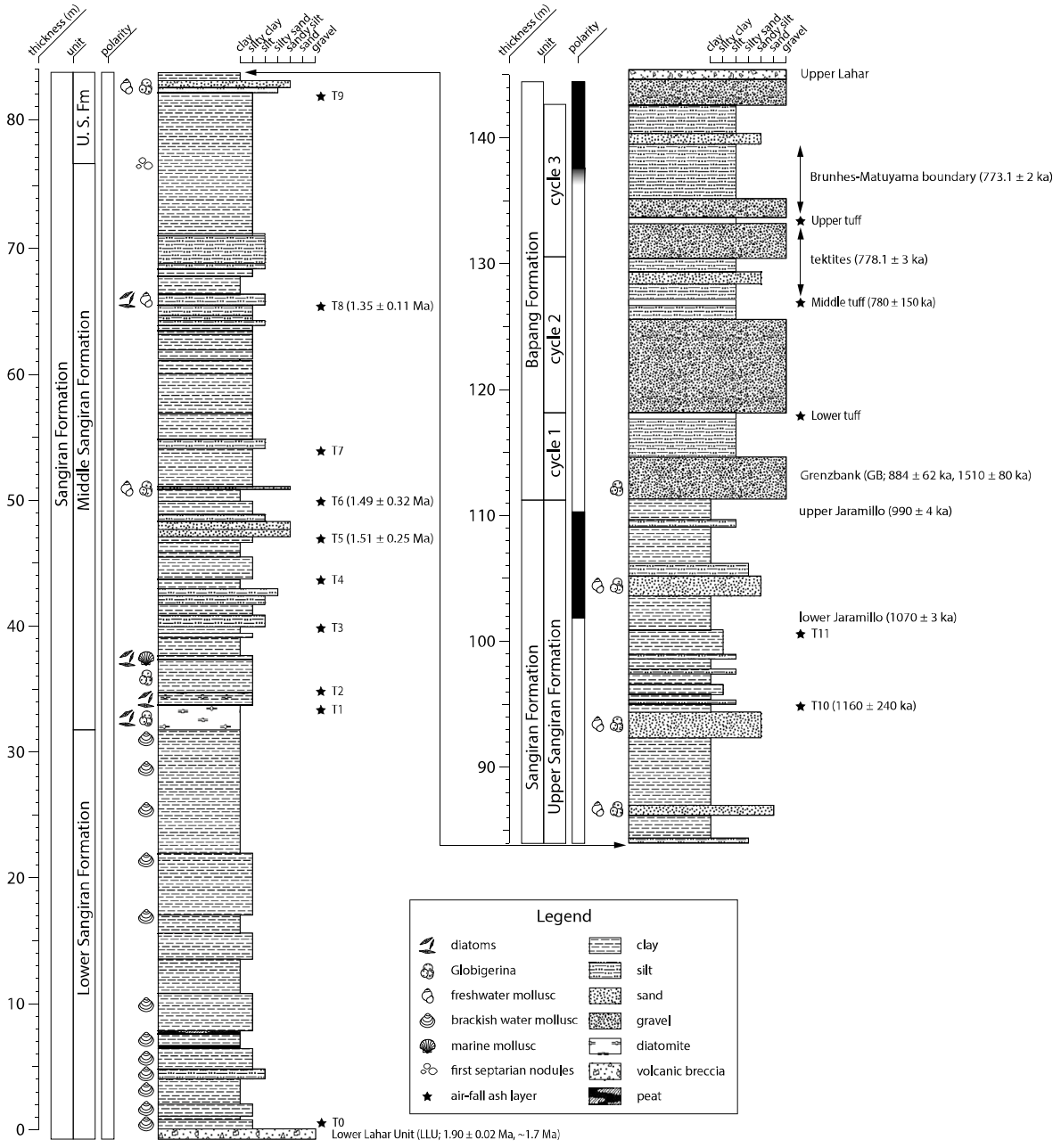

Fig. 2. Combined lithological column of the Sangiran and Bapang Fms. The Sangiran Fm is based on Itihara et al. (1985a, 1985b), Brasseur (2009) and Brasseur et al. (2015), the Bapang Fm on Bettis et al. (2009). Note that the light grey layers (i.e., Lower tuff, Middle tuff and Upper tuff) in the Bapang Fm are air-fall ash layers and have thicknesses associated with them contrary to those in the Sangiran Fm.

field tektites dated at 788.1 ± 3 ka (2σ; Jourdan et al., 2019) were found slightly below this reversal, between the Middle and Upper tuff (Itihara et al., 1985c; Hyodo et al., 2011). Finally, a reverse to normal polarity reversal is identified at ~138 m which could be the start of the Jaramillo normal polarity subchron (1.070 Ma in GPTS2020) assuming a GB age of 1.51 ± 0.08 Ma. Alternatively, assuming a c. 900 ka age for the GB it has been interpreted as the Brunhes-Matuyama boundary (0.773 Ma in GPTS2020, Hyodo et al., 1993, 2011).

Whereas most chronologic markers can be easily correlated between the various stratigraphic sections of the Sangiran Fm this is less straightforward for the Bapang Fm, which shows more variation between the various published stratigraphies. Hyodo et al. (2011) locate the Brunhes-Matuyama reversal c. 2 m above the Upper tuff and the Australasian strewn field tektites are projected between the Middle and Upper (Middle) tuff. Assuming these stratigraphic constraints are correct, the chronologic markers are projected in their respective location within the Bapang Fm stratigraphy presented by Bettis et al. (2009). Note that Larick et al. (2001) do not mention the location or discovery of tektites and consider the claim of in-situ tektites in the Bapang Fm unreliable despite published pictures (Itihara et al., 1985c) and ages (Suzuki et al., 1985).

3. Material and methods

3.1. Stratigraphic column

The Sangiran Dome area has been investigated for a long time resulting in several studies with various levels of detail and focus. One of the most comprehensive stratigraphic studies of the area resulted from fieldwork carried out between 1976 and 1979 as part of the Indonesia-Japan Joint Research Project (IJRCP), which, amongst others, aimed to construct a detailed stratigraphy for the entire Sangiran Dome area. The resulting report, edited by Watanabe and Kadar (1985), remains to date one of the most if not the most detailed stratigraphic study of the Sangiran Dome area. Our study uses the sedimentary log constructed by the IJRCP as the basis for the cyclostratigraphic analysis of the Sangiran Fm, which is the focus of this investigation.

The Sangiran Fm composite stratigraphic column (Fig. 2) was taken from the figures in Itihara et al. (1985a) with some additions from the concluding chapter by Itihara et al. (1985b). We used sections III-2 and 3 near the village of Pablengan for the stratigraphic interval between the LLU and Tuff 2, the section recorded at location IV at the Cemoro Dam site for the interval between Tuff 2 and Tuff 8, section V-2, Pablengan stream, for the interval between Tuff 8 and Tuff 10, and finally section VI near the Mb site for the interval between Tuff 10 and the GB.

For the overlying Bapang Fm (Fig. 2), the stratigraphy published by Bettis et al. (2009) was used as it appears the most suitable for cyclostratigraphic analysis of the Bapang Fm and contains the locations of key chronostratigraphic markers. A comparable stratigraphy with similar regular alternations can be found in Brasseur (2009) and Brasseur et al. (2015).

A semi-quantitative grain size record for the Sangiran and Bapang Fms was then constructed based on the composite stratigraphic column outlined above. All lithologies were assigned a lithological rank based on their grain size. Finer sediments indicative of lower energy conditions in the depositional environment were assigned a lower number and coarser sediments indicative of higher energy conditions were assigned a higher number (clay = 1, silty clay = 2, clayey silt = 3, silt = 4, sandy silt = 5, sand = 6, gravel = 7). Diatomite was assigned a lithological rank of 1. The lithological rank was then used in combination with layer thickness to construct a semi-quantitative grain size record for both the Sangiran and Bapang Fms. The LLU at the base of the Sangiran Fm is interpreted as resulting from the sector collapse of a nearby stratovolcano (Larick et al., 2001). Therefore, due to its atypical, abrupt nature compared to the lagoonal and lacustrine sediments of the rest of the Sangiran Fm, it is excluded from time series analysis. The resultant semi-quantitative grain size record has a resolution at the cm scale. However, small uncertainties in the order of several cm may result from the transfer of the original sedimentary logs to the semi-quantitative record, but these are not large enough to significantly influence the outcome of the time series analysis. For example, 1 cm in the Sangiran Fm would amount to ~68.5 years according to Initial Age Model I (IAM I) and ~34.8 years according to Initial Age Model II (IAM II).

3.2. Age models

Two age models, Initial Age Model I (IAM I) and Initial Age Model II (IAM II), were constructed using two different sets of tie points and correspond to the paleoanthropological short (i.e., a late arrival of *H. erectus*) and long (i.e., an early arrival of *H. erectus*) chronologies, respectively. These initial age models and the tie points on which they are based are discussed in detail in section 4.2. In addition, two different approaches are used to establish these initial age models and apply them to convert the semi-quantitative grain size record into time series for the purpose of cyclostratigraphic analysis, one assuming a constant sedimentation rate (CSR) and one applying a Bayesian age modelling approach (BAY). When necessary and possible the published $^{40}Ar/^{39}Ar$ ages were recalculated for consistency using the same age for the standards and decay constants (see SI Text 1 for a more detailed explanation).

Additionally, time series analysis in cyclostratigraphic studies are often first applied in the stratigraphic domain before conversion to the time domain. The outcome of the time series analysis in the stratigraphic domain will share many similarities compared to the constant sedimentation rate approach but focuses on cycles in terms of their thickness (see also next section 3.2.1).

3.2.1. Constant sedimentation rate

The constant sedimentation rate approach assumes a constant sedimentation rate that is based on the stratigraphically lowest and highest tie point available in the stratigraphic succession. These tie points and the resultant age model were then used to convert the semi-quantitative grain size record into a time series by linear interpolation between and extrapolation beyond the two selected tie points (Interpolation function; version 2.4; Li et al., 2019).

The Sangiran Fm predominantly consists of fine-grained sediments, which have mostly been deposited under low-energy lagoonal and lacustrine conditions that are favorable for near-constant sedimentation rates. A constant sedimentation rate approach is more often employed in cyclostratigraphic studies in which settings with a (near-)constant sedimentation rate might be expected such as deep marine and lacustrine environments (e.g., Olsen and Kent, 1996; Abdul Aziz et al., 2008; Mitchell et al., 2008). Importantly, the IJRCP publication does not provide evidence for the presence of beds indicative of high-energy conditions in the Sangiran Fm such as turbidites, seismites, mass flows and slumps that might be expected in an active volcano-tectonic setting such as Java and which would significantly affect the sedimentation rate. Instantaneous depositional events only occur in the form of relatively thin volcanic ash beds that are occasionally intercalated in the stratigraphic succession of the Sangiran Fm (i.e., “generally thin except for T10 which is 5–20 cm”; Itihara et al., 1985a). The original publications do not mention the thickness of these ash layers in more detail which prevents their removal from the sedimentological logs of the Sangiran Fm. However, due to their limited thickness, this will be of minor influence.

3.2.2. Bayesian age model

Alternatively, a Bayesian age model (BAY) was created that uses the available numerical ages and their stratigraphic position as tie points. To create these Bayesian age models the Bchron package (version 4.7.6; Haslett and Parnell, 2008) in R (version 4.2.0; R Core Team, 2022) was used. Although originally developed for radiocarbon dating, Bchron can also be used with numerical ages obtained from other dating methods (e.g., fission track, $^{40}Ar/^{39}Ar$). Bchron was selected as it is rather conservative in taking uncertainties in the ages of tie points into account; this is considered advantageous as the ages of tie points used in this study are based on widely different methods while it is not clear if full uncertainties have always been considered (i.e., in magnetostratigraphic and U–Pb ICP-MS dating). The Bchronology function was used to convert the tie points into an age model with a spatial resolution of 10 cm. The resulting age model was then used to convert the semi-quantitative grain size record into a time series using the age scale - tuning function in Acycle (version 2.4; Li et al., 2019). A disadvantage for developing Bayesian age models for the Sangiran and Bapang Fms are the relatively large uncertainties tied to many of the numerical age estimates of the tie points.

3.3. Time series analysis

Spectral analysis is commonly used as a quantitative method to detect cycles in sedimentary and paleoclimatic records. First, the time series was, where necessary, evenly resampled to the median sampling resolution and detrended using the locally estimated scatterplot smoothing (LOESS) non-parametric local regression technique to remove long-term trends. These preparatory steps were carried out in Acycle (version 2.4, Li et al., 2019). The Multi-Taper Method (MTM) method with a 2π taper (Thomson, 1982), which is widely applied in paleoclimatic studies to analyze relatively short noisy records, was selected for spectral analysis of the grain size records. The MTM analysis (mtmML96) was carried out in R using the Astrochron package (version 1.1, Meyers, 2014) as it includes the Robust first order auto-regression of Mann and Lees (1996) corrected by Patterson et al. (2014) to calculate confidence levels (CLs). The basic idea of the 'robust' method is to better estimate the 'true' noise model, in records that are suspected to include strong (quasi-)periodic variability. Finally, bandpass filtering of the relevant grain size cycles identified by the MTM spectral analysis was used to localize specific cycles in the depth or time series (Filtering function, Acycle).

4. Results

4.1. Stratigraphic column

The Sangiran Fm composite stratigraphic record (Fig. 2) is characterized by variations in grain size that often appear regular. In the Lower Sangiran Fm, regular grain size alternations with an approximate thickness of 6 m are composed of silt and silty clay; these are especially visible in the lower c. 22 m. In the Middle Sangiran Fm, grain size alternations with a similar thickness are mostly expressed as (silty) clays and (sandy) silts with a single sandy layer at c. 47 m, but alternations on a smaller scale are visible as well. In the Upper Sangiran Fm, the grain size starts to increase slightly further and alternations consist of (silty) clays and (silty) sands. The sand layers are intercalated at regularly spaced intervals of c. 10 m; again, smaller scale alternations are found as well, but these are less coarse and do not contain sands.

The Bapang Fm is much coarser grained and consists of gravels and sands alternating with tuffaceous silts and sands. Bettis et al. (2009) describe just over 3 alternations in c. 33 m of sediment resulting in an approximate thickness of 10 m, similar to the thickness of the principal alternations in the Upper Sangiran Fm. In most of these alternations, thinner, coarser grained layers occur again in the finer facies.

4.2. Age models

Age modelling efforts and time series analysis initially focus on the Sangiran Fm, after which the Bapang Fm will be incorporated. As mentioned before, not all published age constraints are consistent with one another, resulting in two initial age models, IAM I and II, that were used to convert the semi-quantitative grain size record into a time series by means of two different approaches (CSR and BAY). Here these age models and their conversion into timeseries are described in more detail.

4.2.1. Initial age model I

The IAM I CSR age model for the Sangiran Fm is based on an LLU age of 1682 ± 106 ka (2σ; recalculated from Sémah et al., 2000) and an age of 990 ± 3.0 ka for the Upper Jaramillo (2σ; Channell et al., 2020). Taking these two ages into account results in an average sedimentation rate of ~15.9 cm kyr-1, slightly higher than the average sedimentation rate of 13.7 cm kyr-1 originally suggested for the Sangiran Fm by Shimizu et al. (1985). To extend this age model into the Bapang Fm and create a composite, the Upper Jaramillo tie point is replaced by the stratigraphically higher Brunhes-Matuyama boundary in the upper part of the Bapang Fm with an astronomical age of 773 ± 2 ka (2σ; Channell et al., 2020).

The IAM I BAY age model for the Sangiran Fm was constructed using seven tie points: the LLU, T5, T6, T8, T10, and the Lower and Upper Jaramillo (see Table 1 for an overview of the used tie points). For the Jaramillo subchron boundaries an extra uncertainty of ± 1 m was added to their stratigraphic position. Several tie points located in the Bapang Fm were added to IAM I BAY incorporating the Bapang Fm (i.e., GB, MT, BM, tektites, see Table 1). An uncertainty of ± 1.5 m was added to the position of the Brunhes-Matuyama reversal and the Australasian strewn field tektites.

4.2.2. Initial age model II

The IAM II CSR is based on an LLU age of 1917 ± 34 ka (2σ, recalculated from Bettis et al., 2004), and an age of 1529 ± 76 ka for the GB (2σ, recalculated from Larick et al., 2001) (see Table 2 for an overview of the used tie points). The tie points for this initial age model were selected based on their similar dating approach utilizing multigrain hornblende ages from detrital pumice. IAM II CSR suggests a sedimentation rate of ~28.2 cm kyr-1, roughly twice as high as that of IAM I CSR.

For the construction of the IAM II BAY age model, the same two tie points are available as used for the constant sedimentation rate approach and as a result the two age models are nearly identical. This age model was only established for the Sangiran Fm and not extended to incorporate the Bapang for reasons outlined in 4.4.

Table 1
Overview of the ages and stratigraphic heights of the tie points used in Initial Age Model I (IAM I).

tie point	height (m)	age (kyr)	±	2σ	reference
Brunhes-Matuyama boundary	132.8	773	±	2	Channell et al. (2020)
Tektites	126.4	788.1	±	3	Jourdan et al. (2019)
Middle tuff	124.9	780	±	150	Suzuki et al. (1985)
Grenzbank (GB)	112.8	884	±	62	Matsu'ura et al. (2020)
Upper Jaramillo	110.2	990	±	4	Ogg (2020)
Lower Jaramillo	100.1	1070	±	3	Ogg (2020)
Tuff 10	94.3	1160	±	240	Suzuki et al. (1985)
Tuff 8	65.1	1345	±	108	Matsu'ura et al. (2020)
Tuff 6	48.8	1490	±	320	Suzuki et al. (1985)
Tuff 5	47.0	1510	±	250	Suzuki et al. (1985)
Lower Lahar Unit (LLU)	0.0	1682	±	106	Sémah et al. (2000)

Table 2
Overview of the ages and stratigraphic heights of the tie points used in Initial Age Model II (IAM II).

tie point	height (m)	age (kyr)	±	2σ	reference
Grenzbank (GB)	112.8	1529	±	76	Larick et al. (2001)*
Lower Lahar Unit (LLU)	0.0	1917	±	34	Bettis et al. (2004)*

4.3. Time series analysis

4.3.1. Stratigraphic domain

Time series analysis in the stratigraphic domain served as a starting point to detect cycles in the original grain size record. The MTM power spectrum revealed four prominent peaks that correspond to cycle thicknesses of 10.7, 6.0, 3.5 and 1.2 m (Fig. 3A). The 6.0, 3.5 and 1.2 m cycles all reach confidence levels above 99% while the 10.7 m cycle reaches a confidence level between 95 and 99%. Bandpass filtering of the 6.0 and 10.7 m cycles reveals that the 10.7 m cycle abruptly increases in amplitude at ~80 m in the Upper Sangiran Fm where two 6.0 m cycles consistently match one ~10.7 m cycle (Fig. 4).

4.3.2. Initial age model I

Spectral analysis of the IAM I CSR time series yielded four main significant spectral peaks at 67.2, 38.0, 22.3, and 7.7 kyr (Fig. 3C), corresponding to the 10.7, 6.0, 3.5, and 1.2 m cycles in the stratigraphic domain. The 67.2 kyr peak reaches a CL between 90 and 95%, while the other cycles reach CLs above 99%. Spectral analysis of the IAM I BAY time series yielded a single individual peak at 16.5 kyr with a CL above 99% and a broad frequency band corresponding to periods from 30 to 60 kyr with CLs between 90 and 99% (Fig. 3D). The cycle periods obtained from the IAM I CSR time series can rather straightforwardly be related to Milankovitch forcing. The 22.3 and 38.0 kyr cycles match the periods of precession (~21 kyr) and obliquity (~41 kyr) well, while the ~67.2 kyr cycle is too short to be attributed to the ~100 kyr eccentricity cycle. Alternatively, it might represent the ~80 kyr double obliquity cycle, which is well expressed in Pleistocene benthic $d^{18}O$ records, including the LR04 stack (Lisiecki and Raymo, 2005). This cycle rather abruptly increases in strength around 1.2 Ma in the LR04 isotope stack. The 7.6 kyr cycle corresponds well to the average period of the Heinrich events of the late Pleistocene (~7 kyr; Bond et al., 1992), and cyclicity with similar duration has also been observed in older Pleistocene glacials (Becker et al., 2005; Hodell et al., 2008). However, this connection should be considered tentative for the moment.

The IAM I BAY MTM power spectrum is difficult to interpret in terms of Milankovitch cyclicity, as it contains this very broad band with elevated CLs. The single peak at 16.5 kyr might be related to precession although it is too short.

4.3.3. Initial age model II

The results from spectral analysis of the IAM II CSR and BAY time series are almost identical due to the use of the same two tie points. As a result, the MTM power spectra yielded almost identical cycles with periods of 38.0, 20.1, 12.2, 6.2 and 4.2 kyr for IAM II CSR and 37.2, 20.7, 11.4, 7.5, 6.1 and 4.2 kyr for IAM II BAY (Fig. 3E and F). The 38.0/37.2 kyr cycle reaches a CL between 95 and 99%, while all other cycles have a CL above 99% associated with them.

These cycles can also straightforwardly be interpreted in terms of astronomical cycles. The 20.7/20.1 and 38.0/37.2 kyr cycles may correspond to precession and obliquity, while the 11.4/12.2 kyr cycle might reflect semi-precession. The shorter 4.2 kyr cycle occurs in the sub-Milankovitch band of the spectrum, but the period is distinctly longer than that of the Dansgaard-Oescher cycles and shorter than that of the Heinrich events.

4.4. Comparison of the initial age models

Here the results of the time series analysis of the Sangiran Fm grain size record based on the two age models, IAM I and IAM II, are discussed and compared in detail to select the best possible age model. This age model selection is critical to carry out the next steps in this study, namely the inclusion of the Bapang Fm and the astronomical tuning of the grain size record of the Sangiran-Bapang composite.

Spectral analysis of both IAM I and IAM II results in cycles that can be related to Milankovitch cyclicity when assuming a constant sedimentation rate. On the other hand, the IAM II BAY results are nearly identical to those of the IAM II CSR because the same two tie points are used to construct these age models. However, interpreting the IAM I BAY MTM power spectrum in terms of Milankovitch cycles is problematic. The degradation of the peaks in this spectrum and the broad band with high CLs may result from the changes in sedimentation rate inherent to the BAY model and caused by the ages and age uncertainties of the tie points. For this reason, we argue that the CSR models result in a more compelling outcome and are thus more reliable than the BAY models. As mentioned before, both IAM I CSR and IAM II CSR result in a logical outcome in terms of astronomical forcing. However, in case of IAM I, the three main cycles can be related to precession, obliquity, and double obliquity and in case of IAM II to semi-precession, precession and obliquity. The most logical reason for this outcome is coincidence as the Sangiran Fm encompasses approximately twice as much time in IAM I (~700 kyr) compared to IAM II (~400 kyr). However, there is one crucial difference between the two age models. According to IAM I CSR, there is a marked and abrupt increase in the amplitude of the ~67.2 kyr double-obliquity related cycle around ~1.12 Ma. This increase can be related to the onset of the MPT at 1.2 Ma (Head and Gibbard, 2005), where a similar abrupt transition from obliquity to double obliquity is observed in the benthic $\delta^{18}O$ records, corresponding to the marked increase in both amplitude and duration of the ice ages at that time. By contrast, it is difficult to explain a rather abrupt transition from precession to obliquity around the base of the Upper Sangiran Fm at an age of >~1.5 Ma according to IAM II, as no such transition is known around that time. A gradual increase in the strength of the obliquity cycle occurs much earlier at the onset of the major Northern Hemisphere glaciations between ~3.5 and 2.5 Ma (Trauth et al., 2021). Hence, IAM I CSR is considered the most reliable age model as it provides a much better explanation for the abrupt shift in cyclicity observed around the middle to Upper Sangiran Fm boundary.

4.5. Including the Bapang Fm

The Bapang Fm grain size data was added and the preferred IAM I age model again with the constant sedimentation rate as well as the Bayesian age modelling approach was applied to analyze the grain size record of the Sangiran-Bapang composite. This cyclostratigraphic analysis will also start in the stratigraphic domain. This resulted in the detection of two prominent cycles with thicknesses of 10.4 and 6.4 m (Fig. 3B). Additional higher frequency peaks of 3.7 and 3.0 m are also present, together with an even higher-frequency 1.2 m cycle. All cycles have a >99% CL associated with them. The results of bandpass filtering show that the two most conspicuous cycles form the upward continuation of the 10.7 and

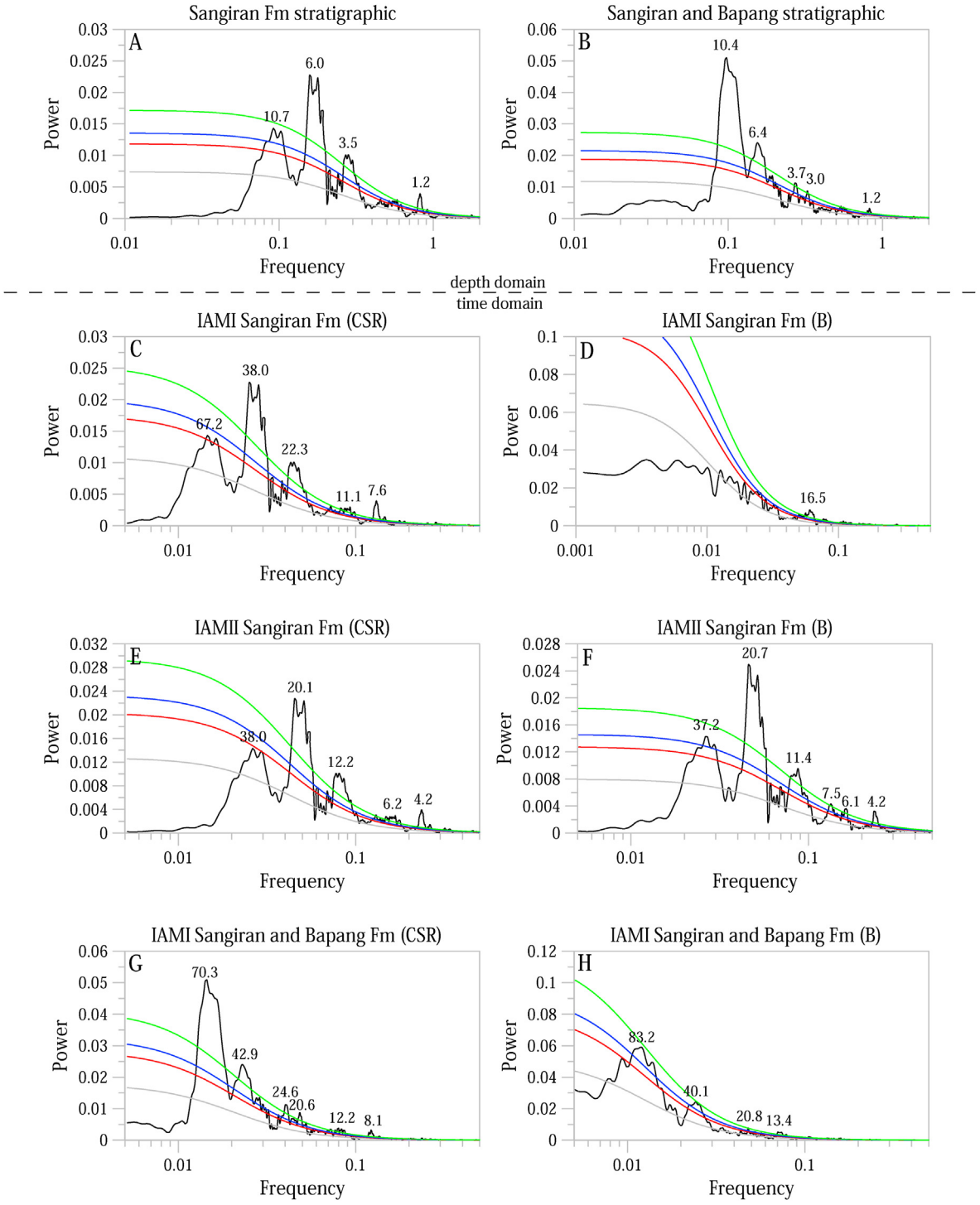

Fig. 3. MTM power spectra of the semi-quantitative grain size records of the depth series of (a) the Sangiran Fm, (b) the Sangiran and Bapang Fms, and the time series of (c) the Sangiran Fm according to IAM I and assuming a constant sedimentation rate, (d) the Sangiran Fm according to IAM I using a Bayesian age modelling approach, (e) the Sangiran Fm according to IAM II and assuming a constant sedimentation rate, (f) the Sangiran Fm according to IAM II using a Bayesian age modelling approach, (g) the Sangiran and Bapang Fms according to IAM I and assuming a constant sedimentation rate, (h) the Sangiran and Bapang Fms according to IAM I and assuming a constant sedimentation rate. Significance levels were calculated using the Robust AR method (Acycle). The black line indicates power, the grey line indicates AR fit, the red line indicates 90% AR1 confidence level, the blue line indicates 95% AR1 confidence level and the green line indicates 99% AR1 confidence level. (For interpretation of the references to colour in this figure legend, the reader is referred to the Web version of this article.)

6.4 m cycles found in the Sangiran Fm, despite the slight difference in thickness (Fig. 4).

The MTM power spectrum of the Sangiran-Bapang grain size record based on IAM I CSR is shown in Fig. 3G. It reveals two main peaks corresponding to periods of 70.3 and 42.9 kyr and confidence levels >99%, with additional higher frequency peaks at 24.6, 20.6, 12.2 and 8.1 kyr and confidence levels of >99% as well. These cycles correspond with the cycles observed in the stratigraphic domain.

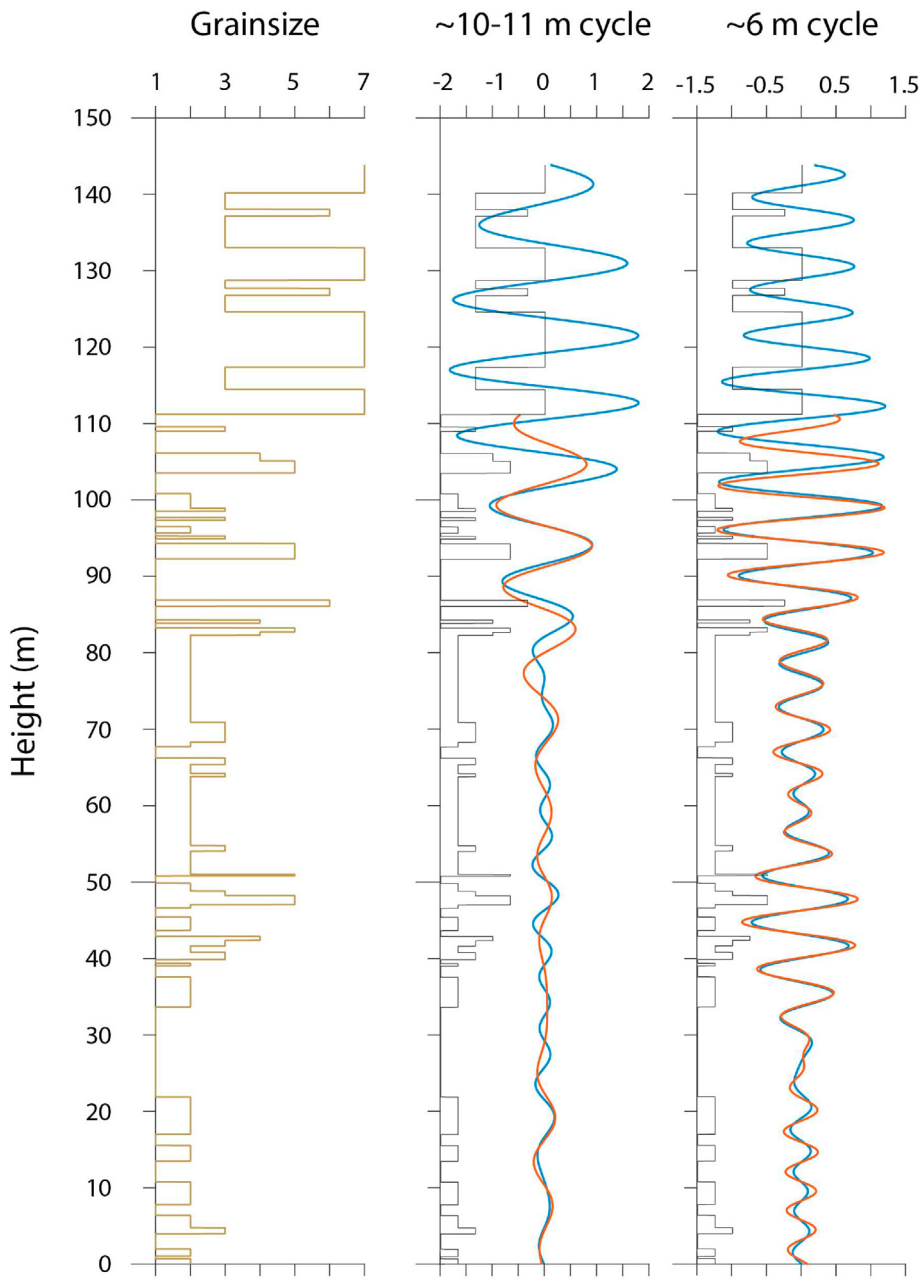

Fig. 4. Bandpass filtered cycles projected onto the semi-quantitative grain size record (light grey). (a) semi-quantitative grain size record (b) the ~9.3–11.3 m cycle in the Sangiran Fm (red line; filter frequency: 0.135–0.2) and Sangiran and Bapang Fm (blue line; filter frequency: 0.138–0.185). (b) the ~6.0–6.2 m cycle in the Sangiran Fm (red line; filter frequency: 0.07–0.11) and Sangiran and Bapang Fm (blue line; filter frequency: 0.083–0.135). (For interpretation of the references to colour in this figure legend, the reader is referred to the Web version of this article.)

Overall, the outcome shows a similarly good fit with the periods of Milankovitch cycles as compared to the results of the Sangiran Fm only. Moreover, bandpass filtering of the two main peaks - at 70.3 and 42.9 kyr - in the MTM power spectrum reveals that the same two cycles are identified in the stratigraphic domain (Fig. 4). These results further suggest that the ~67.2 kyr cycle in the Upper Sangiran Fm smoothly continues in the younger Bapang Fm. From a cyclostratigraphic perspective, this suggests that the succession is either essentially continuous across the formational boundary or that – given the independent age constraints for IAM I – approximately one ~70.3 kyr cycle (~10 m) has been eroded. The presence of a depositional hiatus between the Sangiran Fm and the Bapang Fm will be further explored in section 5.1.

The MTM power spectrum based on the IAM I BAY age model reveals two broad peaks corresponding to periods of 83.2 and 42.9 kyr with confidence levels between 95 and 99% (Fig. 3H). In addition, higher frequency peaks at 20.6 and 13.4 kyr and confidence levels of >99% were detected.

These peaks correspond well to double-obliquity, obliquity, precession, and semi-precession. However, like the Bayesian age modelling approach for the Sangiran Fm only, the spectrum appears affected by the changes in sedimentation rate implied by the Bayesian age model, which likely explains the broadness of the two main peaks. This complexity is further illustrated by the results of bandpass filtering of these two cycles according to the CSR and BAY approaches, as outlined in detail in the SI Text 2 and SI Figure 1.

Summarizing, the filters mainly pick up the clear alternations in grain size that correspond to the 6 and 10.7 m cycles in the stratigraphic domain, but the number of cycles may differ, sometimes considerably, between these age models in specific intervals. These differences can best be explained by the changes in sedimentation rate implied by the Bayesian age model of which it is unclear whether they are real or not in view of the large uncertainties in the ages of most of the tie-points used in IAM I BAY. Thus, like for the Sangiran Fm, the outcome of the time series analysis again suggests that the use of the IAM I BAY for the Sangiran-Bapang composite is less reliable than the IAM I CSR. Nevertheless, the outcome of this age model is also consistent with linking the 6.0 and 10.7 m cycles to obliquity and double obliquity. Yet, we will use the results of the IAM I CSR S + B age model as starting point for our attempt to astronomically tune the cycles.

5. Astronomical tuning

If the main 42.9 and 70.3 kyr grain size cycles in the Sangiran and Bapang Fms according IAM I CSR are indeed controlled by obliquity and double obliquity, the question is whether these cycles can be used to establish an astronomical age model for the Sangiran and Bapang Fms by correlating or tuning them to an astronomically derived target curve.

Rather than using a combined precession-obliquity (PT) or insolation curve (e.g., 65°Nlat summer insolation), the LR04 benthic $\delta^{18}O$ isotope stack (Lisiecki and Raymo, 2005) was selected as the underlying age model is based on correlating the LR04 stack to the outcome of an astronomically forced ice volume model. However, the main reason to select the LR04 stack as target curve is that it contains a strong record of ice age history, including the sudden appearance of the double obliquity cycle at the onset of the MPT, which seems to be recorded in the Sangiran and Bapang Fms as well. This ~80 kyr cycle, which is not present in the astronomical solution itself, has been explained by a non-linear or stochastic response of the climate system to astronomical forcing and the dominant obliquity induced ice ages (Huybers, 2009; Lourens et al., 2010). Consequently, it is not present in insolation or other target curves, which are solely based on the astronomical solution itself, making them less suitable for our tuning.

An important aspect of astronomical tuning is the phase relation between the cycles in the semi-quantitative grain size and the LR04 benthic $\delta^{18}O$ isotope record. Thus, the question is whether the finer or coarser-grained beds are related to obliquity-induced glacials or interglacials and hence to low or high glacio-eustatic sea-level stands. Here it is assumed that the finer sediments are related to interglacial periods and coarser sediments to glacial periods. The full implications of - and motivation behind - this phase relation are discussed in section 6.1. Below two astronomically tuned age models using IAM I CSR as starting point are presented.

5.1. Astronomical age model I

Astronomical Age Model I (AAM I; Fig. 5) is based on correlating the first "strong" ~70.3 kyr cycle at 1.12 Ma to the first distinct double obliquity cycle in the LR04 stack (MIS 36 at ~1.2 Ma). Continuing upward the two upper coarse sand layers in the Upper Sangiran Fm are tuned to MIS 34 and MIS 30, respectively. Next, successively older ~42.9 kyr cycles were tuned to their correlative MIS. The resultant astronomical ages are in good agreement with all the fission-track ages. Following this tuning downward results in the first layer of coarser sediments directly above the LLU to correlate with MIS 66 at c. 1.82 Ma, somewhat older than the ~1.7 Ma suggested by Sémah et al. (2000). Based on this tuning, the youngest part of the Olduvai normal polarity subchron (1.925–1.77 Ma; Ogg, 2020) should be recorded in the lowermost part of the Sangiran Fm. However, the Olduvai subchron is either placed below the LLU in the marine Puren Fm (Shimizu et al., 1985) or in the LLU itself (Sémah et al., 2000). Thus, the existing magnetostratigraphy of the Lower Sangiran Fm disagrees with this astronomically tuned age model.

Tuning the Bapang Fm under this scenario leads to two different tuning options, one with and one without a significant hiatus between the Sangiran and Bapang Fms. Firstly, assuming no erosional hiatus, the tuning outlined above for the Sangiran Fm would result in correlating the GB to MIS 26 and the three ~70.3 kyr cycles above it to MIS 22, MIS 20 and MIS 18 (Fig. 5). This is at odds with Matsu'ura et al. (2020), who link the Grenzbank to MIS 22. This leads to a second possible tuning option that explains this apparent discrepancy as a result a c. 80 kyr erosional hiatus between the Sangiran and Bapang Fm, created by the removal of ~10.7 m of sediment. In this case, the GB is correlated to MIS 22 as suggested by Matsu'ura et al. (2020) and the three subsequent ~70.3 kyr cycles in the Bapang Fm to MIS 20, MIS 18, and MIS 16.

The AAM I tuning option without significant erosion is consistent with the Brunhes-Matuyama reversal boundary being correctly positioned in MIS 19/20. However, it is inconsistent with the inferred position of the Australasian strewn field tektites between the Upper (UT) and Middle tuff (MT) which would be incorrectly placed in MIS 21. For the AAM I option with hiatus, it is the other way around with the Brunhes-Matuyama reversal boundary incorrectly placed in MIS 17/18 and the Australasian strewn field tektites being correctly positioned in MIS 19 (e.g., Hyodo et al., 2011; Mark et al., 2017).

5.2. Astronomical age model II

AAM II (Fig. 6) is based on the same interpretation of the cycles in terms of their duration and origin as in AAM I. The starting point for this astronomical tuning is the best possible fit between the cycle patterns in the semi-quantitative grain size record (especially that of the Sangiran Fm) and the LR04 benthic $\delta^{18}O$ record (Lisiecki and Raymo, 2005).

The best pattern fit starts with the upper three thick and coarse sand layers at c. 85, 93 and 104 m that are correlated to MIS 34, 30, and 26, respectively. In this scenario, the lowest sand layer at c. 85 m consists of two separate sand layers which is in agreement with the shorter interval between MIS 34 and MIS 32. Although some grain size variation is visible, no coarse-grained sediment (i.e., sand) is found between the coarse sand layers that are linked to MIS 30 and MIS 26. This lack of a distinct glacial signal is again consistent with the benthic $\delta^{18}O$ record where MIS 28 lacks the major shift to extreme $\delta^{18}O$ values as seen in the preceding MIS 30 and the succeeding MIS 26. Based on this pattern fit, the fine-grained sediments between the uppermost sand layer at c. 104 m in the Sangiran Fm and the Grenzbank would correspond to MIS 25 to MIS 23 with the GB itself corresponding to MIS 22, as previously suggested by Matsu'ura et al. (2020). Consequently, this astrochronological age model suggests that little or no erosion took place between the Sangiran and Bapang Fm.

At the Middle to Upper Sangiran Fm boundary at c. 77 m, a coarse layer is missing, which according to AAM II is correlated to MIS 35, a c. 80 kyr long interglacial interval lacking a distinct ~41 kyr glacial in the middle. Furthermore, in this scenario, two important indicators for increased marine influence, a marine diatomite at ~34 m and (marine) shell bed 1 at ~38 m are correlated

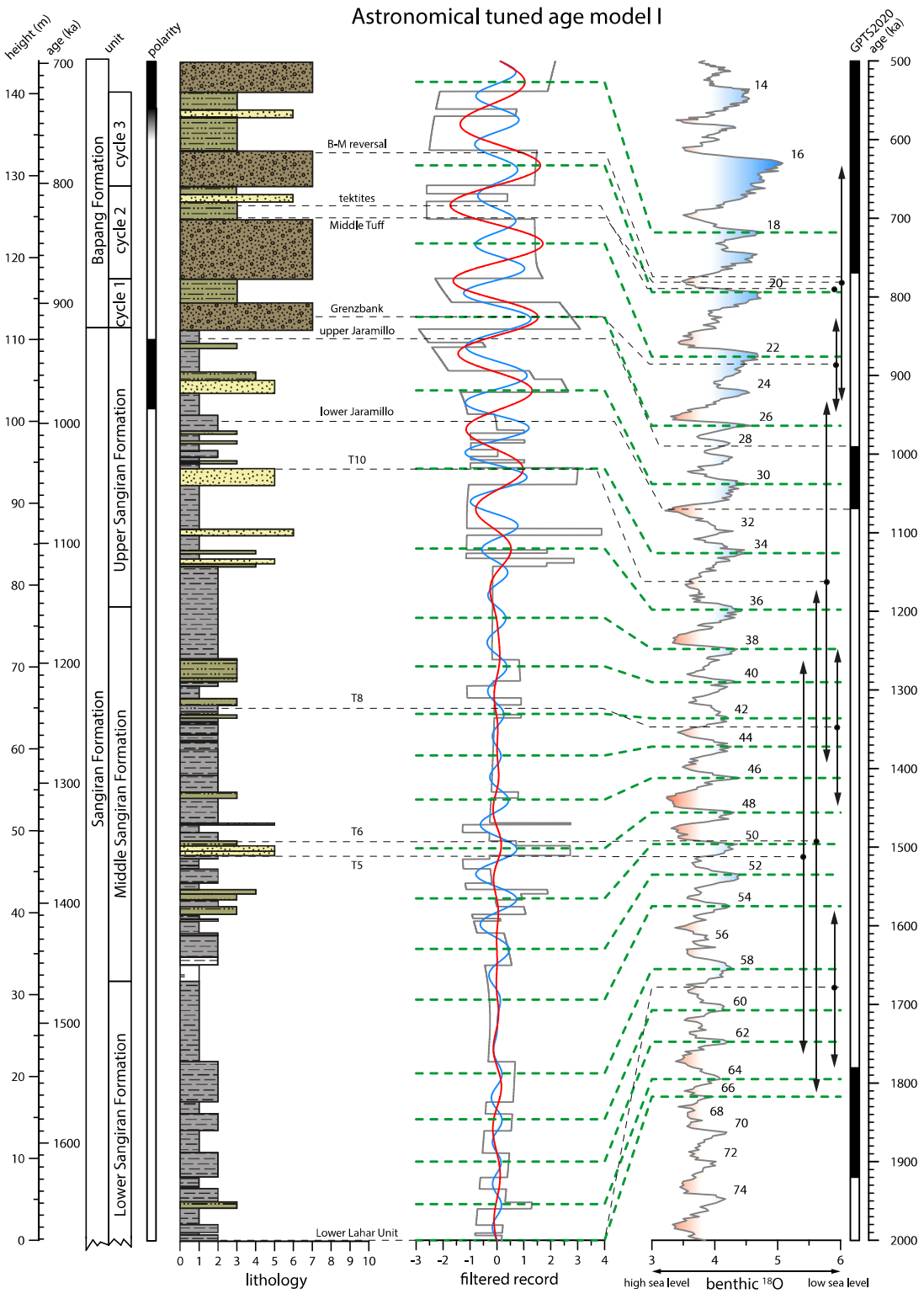

Fig. 5. Astronomically tuned age model I (AAM I) of the Sangiran and Bapang Fms and the tuning to the LR04 benthic $\delta^{18}O$ isotope stack showing the ~64 kyr cycle interpreted as the ~80 kyr double obliquity cycle and the ~41.7 kyr cycle interpreted as the ~41 kyr obliquity related cycle. The increases in intensity of the ~64 kyr cycle in the top of the Sangiran Fm interpreted as the start of the Middle Pleistocene Transition (MPT) was used as a starting point. Thin red dashed lines indicate the correlation of the semi-quantitative grain size record to the LR04 stack. Dashed black lines indicate the position of dated volcanic ash layers, Grenzbank (GB), and magnetic reversals (indicated in the magnetostratigraphic column left of the sedimentary log) and the link to their U–Pb, astronomical or fission track ages, including their uncertainty (indicated by the vertical lines with double arrowheads, left of the polarity time scale on the right). Numbers next to the LR04 stack specify the marine isotope stages in the isotope stack. (For interpretation of the references to colour in this figure legend, the reader is referred to the Web version of this article.)

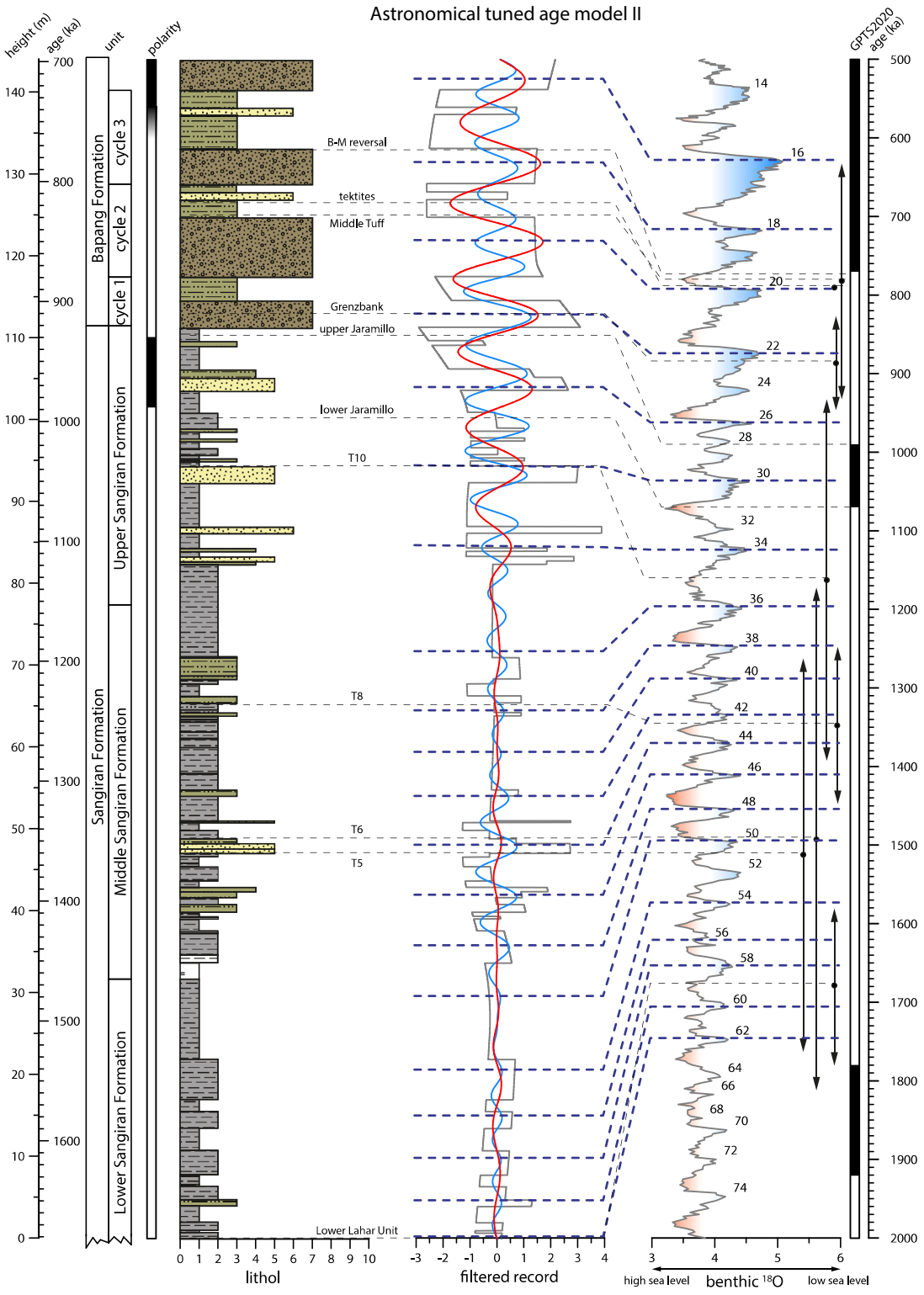

Fig. 6. Astronomically tuned age model II (AAM II) is based on the tuning of the filtered semi-quantitative grain size record to the LR04 benthic $\delta^{18}O$ isotope stack. The AAM II is based on the best fit of the cycle pattern in the semi-quantitative grain size record and the associated changes in lithology including sedimentary and fossil attributes to the LR04 stack (Lisiecki and Raymo, 2005). For further information see the caption of Fig. 5.

to two 'extreme' interglacial periods, MIS 49 and MIS 47, respectively. Interestingly, between these two marine beds, freshwater diatoms are found (Khustina et al., 2014), suggesting a decrease in marine influence possibly as a result of the sea level drop associated with MIS 48. Following the correlation scheme outlined above, the coarser sediment directly above the LLU would correlate with MIS 62 at c. 1.75 Ma, in agreement with the ~1.7 Ma suggested for the LLU by Sémah et al. (2000). Although the observed pattern in grain size variation generally fits well with the pattern in the LR04 stack, there are also some exceptions. For example, glacial stages MIS 50 and 52 do not correspond to increases in grain size, and the same holds for MIS 40. The thin sand at c. 51 m marks a minor deviation in the opposite direction as it is correlated to interglacial MIS 43.

The tuning of the Bapang Fm according to AAM II is identical to that of the AAM I with the depositional hiatus at the base of the GB, being consistent with the position of the Australasian strewn field tektites but inconsistent with that of the Brunhes-Matuyama reversal. The option of AAM II with a marked hiatus at the base of the GB is not considered as this would result in a marked increase in the discrepancies with the independent age constraints.

With the construction of the AAMs, all age models can now be compared with one another. This comparison is included in the SI (SI Text 3) as it is partly a summary and repetition of what has been mentioned before.

6. Discussion

The results of our cyclostratigraphic study provide arguments that the grain size cycles in the Sangiran and Bapang Fms are astronomically controlled. However, other processes may have played a role as well and can provide alternative explanations for the formation of the cycles. One possible explanation is that these cycles are not controlled by allogenic but by autogenic processes that occur within the sedimentary system itself. Generally, it is assumed that such processes operate on shorter time scales, but a recent paper suggested that they may occur on longer Milankovitch time scales as well (Hajek and Straub, 2017), providing an alternative mechanism to astronomical climate control for the formation of fluvial floodplain sequences in the early Paleogene of North America (Abdul-Aziz et al., 2008; Abels et al., 2013). Such autogenic variability in fluvial systems may also control the regular cyclic alternations in the Sangiran Fm if the somewhat coarser grained beds in these alternations are related to variations in fluvial input, which is likely the case. Alternatively, the alternations may result from (volcano-)tectonic induced changes in stress regime. However, typical sediment types associated with this process (e.g., Hou et al., 2020) have not been described from the Sangiran and Bapang Fms as mentioned before. Moreover, these alternative scenarios have difficulties in explaining the presence of cycles in the Milankovitch frequency band and the observed cycle hierarchy observed in the Sangiran Fm. This is the especially the case as this hierarchy makes sense in terms of astronomical climate forcing with periods corresponding rather well to obliquity and double obliquity at the same time that these same two cycles exert a dominant control on the ice ages.

However, accepting a Milankovitch control for the hierarchical cyclicity observed in the Sangiran, the presence and nature of these cycles detected through spectral analysis and the phase relation with respect to the astronomical parameters of critical importance for the tuning (see section 5.2) need to be discussed. Several possible mechanisms will be explored before a more detailed depositional model is presented based on the most likely phase relation. Finally, we will discuss some of the implications that result from the application of the astronomical age models in reconstructing hominin history.

6.1. Phase relation and depositional model

Here three different scenarios for explaining the influence of obliquity on the grain size in the Sangiran Dome area stratigraphic record are presented. All these scenarios assume that the ~6.0–6.4 and ~10.4–10.7 m cycles correspond to obliquity and double-obliquity cycles as discussed before (see section 5). The first scenario assumes a direct influence of obliquity on regional climate, while the other two scenarios assume an indirect influence through the Ice Ages. First, the two alternative scenarios to the one preferred in this paper are described. These comprise the direct influence of obliquity on the monsoon independent of the Ice Ages (section 6.1.1), and the indirect influence of obliquity on regional climate (i.e. precipitation) on Java through the ice ages (section 6.1.2). Finally, the preferred scenario, which implies base-level variations resulting from glacio-eustatic sea-level change and a phase relation with the coarser parts of the cycles corresponding to glacial periods and, hence, obliquity minima, is presented (section 6.1.3).

Although the above scenarios all start from allogenic variability, there remains the possibility that other, autogenic processes and cycles in grain size variation play a role as well. These should not be overlooked, although they would likely mostly occur on shorter timescales. In addition, long-term allogenic control, such as (long-term) tectonic uplift or sediment influx related to volcanic activity, will occur at the same time.

6.1.1. Direct influence of obliquity on monsoon

Obliquity exerts a direct control on low-latitude monsoonal climate as suggested by Reichart (1997) and Leuschner and Sirocko (2003), and recently confirmed by climate modelling (Bosmans et al., 2015, 2018). In this scenario, obliquity maxima result in monsoonal intensification, which might explain the coarser-grained part of the ~6.0–6.4 m cycles in the Sangiran Fm as a consequence of enhanced run-off and the resulting increase in terrigenous input. This scenario thus assumes a fast, direct response of the regional low-latitude climate to obliquity.

Interestingly, and in contrast to the general considerations outlined above, climate modelling results for Java consistently reveal a slight reduction rather than the anticipated increase in boreal summer precipitation during obliquity maxima (Bosmans et al., 2018, see their Fig. 3). As a result, the phase relation with coarse grain sizes corresponding to obliquity minima might become opposite and thus similar to the phase relation outlined in our preferred scenario (section 6.1.3), with coarser grain sizes related to obliquity minima, although with a direct (i.e., non-lagged) response to obliquity. However, an important complication is that obliquity maxima may also lead to enhanced austral summer (i.e., December to February) precipitation since obliquity has, in contrast to precession, the same effect on seasonality on both hemispheres. Unfortunately, the modeled changes in austral summer precipitation are not shown, while most precipitation in Indonesia is related to the northeast monsoon and falls from November to March. However, in both cases, a dominant precession induced signal would be expected as precession usually exerts a stronger (direct) influence on monsoonal intensity than obliquity (Bosmans et al., 2015, 2018), but this is not consistently seen in the outcome of the climate models for Java (Bosmans et al., 2018). Nevertheless, the apparent stronger influence of obliquity compared to precession in the Sangiran Fm makes this scenario less likely, also because it fails to explain the sudden shift to the double obliquity related cycle visible in the Upper Sangiran Fm. Note that the climate models do not take ice ages and the resulting reduction in sea surface area due to glacio-eustatic sea-level fluctuations into account. Interestingly a dominant precession signal was suggested

by IAM II (see 4.2.2). However, this option was not further considered, as it is largely incompatible with the most reliable independent age constraints (see 4.4).

6.1.2. Indirect influence of obliquity on monsoon

A second scenario involves the indirect influence of obliquity-induced ice ages on regional climate. In general, one might expect wetter conditions during interglacials and drier conditions during glacials. Such a remote influence of obliquity induced ice ages on low (er) latitude climate has been well documented by aeolian dust flux records from North Africa which reveal a marked increase in obliquity forcing after 2.8 Ma associated with the onset of major northern hemisphere obliquity-controlled glaciations (deMenocal et al., 2000; Tiedemann et al., 1994). Interestingly, these records also reveal a marked shift from obliquity to double obliquity at 1.2 Ma. However, the Sunda shelf likely plays an important role in the Indonesian regional climate. For example, the Sunda shelf mechanism proposed by DiNezio and Tierney (2013) suggests that the shallow Java Sea emerged during periods of sea-level low stands and submerged during periods of sea-level high stands. The submergence of the Sunda shelf during interglacial periods and the resultant increase of the sea surface area results in enhanced precipitation over Java. During glacial conditions, the reverse occurs with a marked decrease in evaporation above the exposed Sundaland (see Fig. 1A), resulting in drier conditions on Java. This change in precipitation amount would result in an increase in river runoff and associated sediment erosion, transport, and deposition during interglacial periods. This scenario would thus result in a phase relation that is opposite to our preferred scenario with fine sediments corresponding to glacial periods (obliquity minima) and coarser sediments with interglacial periods (obliquity maxima). Alternatively, Sarr et al. (2019a) used climate models with different boundary conditions to show that the emergence of the Sunda shelf will result in enhanced convergence and local atmospheric convection, thereby increasing local precipitation during glacials. However, it is not clear whether the increased precipitation may have reached Java. Note that a scenario based on the climate modelling efforts of Sarr et al. (2019a) would result in an identical phase relation between the grain size cycles and the astronomical forcing as our preferred scenario based on the indirect influence of obliquity through sea-level change (see section 6.1.3), including the lagged response relative to obliquity. Interestingly, a recent study suggested that the Sunda Shelf might have been permanently exposed until c. 400 ka/MIS 11 (Sarr et al, 2019b; Husson et al., 2020), ruling out that the aforementioned scenarios, which involve the periodic emergence-submergence of the Sunda Shelf as a consequence of glacio-eustatic sea-level change, are responsible for the grain size cycles in the Sangiran and Bapang Fm during the Early and early Middle Pleistocene.

6.1.3. Indirect influence of obliquity through sea-level change

Our preferred scenario (or conceptual model) explaining the occurrence of astronomically forced cycles in the Sangiran Fm is based on an indirect link between grain size variation and obliquity-controlled ice ages through glacio-eustatic sea-level oscillations (Fig. 7). These sea-level changes in the order of 10 to several tens of meters will have a significant influence on base-level. This scenario prescribes a phase relation where finer grain sizes correspond to interglacial periods and hence obliquity maxima and coarser sediments to glacial periods and obliquity minima. During interglacial periods and associated sea-level high stands, a higher base level results in a decrease in erosion and the deposition of fine-grained sediments (Fig. 7A). During glacial periods, base-level lowering results in enhanced erosion, and terrigenous transport and input of clastics into the basin (lagoon/lacustrine), as expressed by coarser grain sizes (Fig. 7B). Such base-level changes will at the same time also affect local groundwater levels, potentially resulting in local drying during glacials which in turn affects vegetation on a local, but not regional scale. Furthermore, extreme interglacial periods and associated maximum sea levels may even result in a direct marine influence in the Sangiran area as indicated by the presence of layers containing marine species and the presence of pollen indicative of extensive mangrove swamps. Evidently, obliquity-induced glacio-eustatic sea-level variations exerted a major influence on depositional environments in the shallow marine realm at that time, as is convincingly shown in the study of

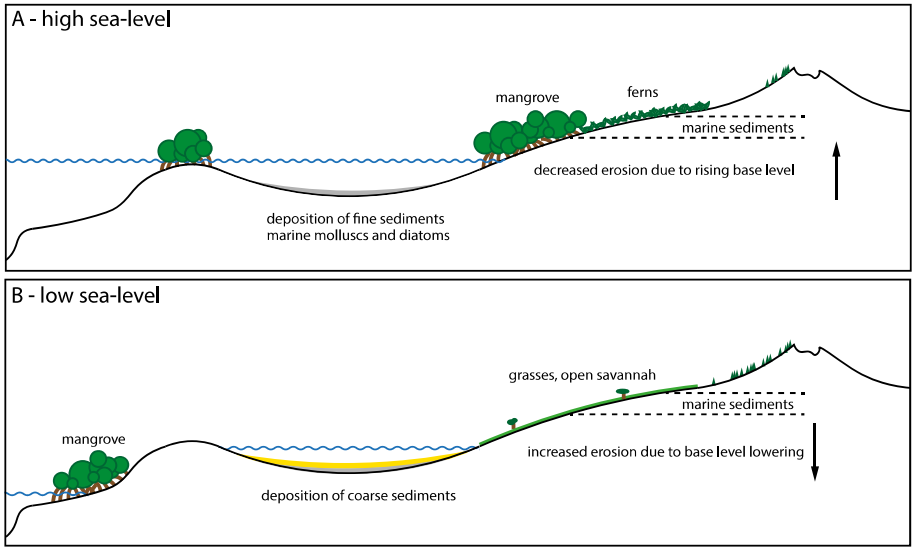

Fig. 7. Depositional model for the Sangiran and Bapang Fm. (a) Interglacial periods with associated sea-level high stands result in decreased erosion due to higher base levels, leading to the deposition of fine-grained sediments. Occasionally, this results in fully marine conditions as evidenced by the marine mollusks and diatoms. (b) During glacial periods the associated sea-level low stands result in increased erosion due to base level lowering causing deposition of coarse-grained sediments. In the Upper Sangiran Fm., older marine sediments are eroded in the hinterland as can be seen by the presence of reworked foraminifera. Potential change in vegetation between glacial and interglacial periods may further influence erosion rates.

Lower Pleistocene cyclothems in the Wanganui Basin in New Zealand (Naish et al., 1998; Naish and Kamp, 1997). In addition, the succession in the Wanganui Basin also reveals the sudden increase in the duration of the glacial cycles from ~41 kyr to ~80 kyr at c. 1.2 Ma.

The two higher frequency cycles, with ~1.2 and ~3.7 m periods are more difficult to interpret. The ~3.7 m cycle (~23–26 kyr) may reflect the influence of the precession cycle through its influence on the low-latitude monsoonal system. Such a monsoonal influence was also attributed to the ~6.0 m cycle in the case of IAM II that was abandoned in favor of IAM I, because of its worse fit with the independent age constraints. However, the response of the monsoon in Indonesia to precession forcing (and thus the phase relation of this cycle with precession) remains problematic as the precipitation change during boreal summer in Indonesia is not fully consistent between models, as already mentioned before (Bosmans et al., 2015, their Fig. 3; see also 6.1.1), while precession-induced precipitation changes are again not shown for austral summer as this study focused on the Indian and East Asian monsoonal response to astronomical forcing. Alternatively, the ~3.7 m cycle may correspond to the first (artificial) harmonic of the ~6.0 m obliquity related cycle or to the sum frequency of the ~10.7 and ~6.0 m cycles (e.g., 1/10.7 + 1/6.0 = 1/3.8). The ~1.2 m cycle (~7.7–8.6 kyr) could be the result of high-frequency noise or reflect high-frequency climate change, as it occurs on the same timescale as the Heinrich events of the last glacial cycle (e.g., Heinrich, 1988), which have now also been detected in older glacials of Pleistocene age, such as MIS 100 (Becker et al., 2005). Alternatively, it might also be of autogenic influence.

6.2. Implications

The astronomical age model(s) presented in this paper have important implications for the chronology of the Sangiran and Bapang Fms, even though multiple tuning options are still possible. Although not definite it serves as an example of their potential for establishing a high-resolution framework for dating the stratigraphic succession at the Sangiran Dome area and to accurately determine ages of hominin history recorded at this site.

Firstly, the tuned ages are mostly consistent with the short paleoanthropological chronology, while they are inconsistent with the long chronology. Besides, astronomical ages for the Middle to Upper Sangiran boundary arrive at either ~1.24 Ma (AAM I) or at ~1.16 Ma (AAM II). This boundary is potentially the oldest possible first occurrence date for *H. erectus* at Sangiran based on the transition from a wetter marshy environment to drier environmental conditions (Brasseur et al., 2015). Matsu'ura et al. (2020) provide an age estimate of ~1.27 Ma for the same boundary based on linear interpolation of the age of the GB tuff (0.884 ± 0.031 Ma, 1σ) and that of Tuff 8 (1.345 ± 0.108 Ma, 1σ). They further mention a maximum age of 1.45 Ma for this boundary based on the maximum fission-track age of Tuff 8. Our oldest possible astronomical age estimate of ~1.24 Ma (AAM I) is consistent with the youngest age estimate of ~1.27 Ma of Matsu'ura et al. (2020) for the boundary, while our alternative astronomical age of ~1.16 Ma of AAM II is somewhat younger. Evidently, astronomical age models have the potential to precisely locate the onset of the MPT defined by the lengthening of the duration of the Ice Ages and their increase in amplitude.

Likewise, the astronomical age estimates for the GB are either 0.965 Ma (MIS26, i.e., AAM I without hiatus) or 0.875 Ma (MIS 22; AAM I with hiatus or AAM II). The exact age of the GB is important in the debate regarding the change from an archaic to a more derived form of *H. erectus* on Java (Kaifu et al., 2010; Kaifu, 2017; Matsu'ura et al., 2020). The younger of these two ages is in agreement with the tentative link of the GB to MIS 22 by Matsu'ura et al. (2020). If so, this would imply that the tuning option according to AAM I without significant erosion at the base of the GB is incorrect. However, as with most of the independent age estimates available in the literature (and potentially also with our astronomical ages), there are some issues related to the ages published by Matsu'ura et al. (2020; see SI Text 3).

A high-resolution astronomically tuned age model might not only help to further constrain the potential first occurrence date for *H. erectus*, but also other species' arrival on Java. For example, the biostratigraphic framework of Java is centered around the supposed periodic influx of "new" species from the SE Asian mainland (Sondaar, 1996; van den Bergh et al., 2001; Volmer et al., 2019). These migration waves are assumed to take place across an emerged Sundaland and are related to an intermittent connection between the SE Asian mainland and the Indonesian islands resulting from emerged or submerged Java Sea caused by glacio-eustatic sea-level change. Although recent studies paint a more complex picture (e.g., Sarr et al., 2019b; Husson et al., 2020; see also 6.1), a higher-resolution framework might answer questions regarding the settling of individual species on Java.

An important question that arises from the hypothesis that obliquity-induced ice ages are responsible for the Sangiran grain size cycles through base-level lowering is whether these ice ages may also have exerted a direct influence on regional climate. Interestingly, the palynological record of the Lower Sangiran Fm (Sémah and Sémah, 1985) reveals quite regular alternations in grasses and sedges in the lower part of the Sangiran Fm on a similar scale as the ~6.0–6.4 m cycle found in this paper. If the scenario presented in this paper is correct, and grain size variation mainly results from glacio-eustatic sea-level fluctuations, the responsible obliquity-induced ice ages may potentially also have resulted in drier and wetter conditions. Thus, these variations in pollen may present a first tentative link between global climate change and the Pleistocene paleoenvironment on Java also experienced by *H. erectus*, although the studied pollen interval precedes the first occurrence of the species at the Sangiran locality.

7. Conclusion

The existing age models for Pleistocene Java are insufficient to test potential links between the hominin population on Java, regional and global climate change, and the paleoenvironment. For this reason, it is necessary to develop high-resolution astronomically tuned age models for the hominin-bearing deposits of Java, specifically those of the Sangiran Dome area. For this purpose, this study aimed to test whether regular alternations in grain size in the Sangiran and Bapang Fms are cyclical and to determine their duration and potential relation to the global climate record, more specifically to known cycles of climate forcing (e.g., ~21 kyr precession, ~41 kyr obliquity, and ~100 kyr eccentricity). The following conclusions can be drawn from our cyclostratigraphic study of the Sangiran and Bapang Fms in the Sangiran Dome area:

- Spectral analysis reveals cyclic variations in grain size with thicknesses of ~10.7, ~6.0, ~3.5, and ~1.2 m within the Sangiran Fm in the stratigraphic domain.
- According to the preferred Initial Age Model I, the four well-defined sedimentary cycles in the Sangiran Fm span ~70.3, 38.0, 22.3 and 7.6 kyr, respectively.
- These sedimentary cycles likely reflect obliquity-induced glacial cycles and associated base-level lowering resulting from glacio-eustatic sea-level change.
- Interestingly, the abrupt transition from obliquity to double obliquity induced glacials at ~1.2 Ma, the onset of the MPT,

seems to be reflected in the Upper Sangiran Formation as suggested by the sudden increase in strength of the ~70.3 kyr cycle, which appears to continue in the overlying Bapang Formation.
- Two astronomically tuned age models are feasible based on either the best fit with available chronological constraints or the best pattern fit with the LR04 benthic $\delta^{18}O$ isotope stack.
- Although more research is necessary to distinguish between these two astronomically tuned age models, this study provides the first step towards a higher-resolution age model for the Sangiran Dome Area.
- Our results are largely consistent with the paleoanthropological short chronology which places the first appearance datum of *Homo erectus* at Sangiran at ~1.2 Ma, coinciding with the onset of the MPT when both the period and amplitude of the glacial-interglacial cycles start to increase.

Author contributions

Sander Hilgen: Conceptualization, Formal analysis, Writing – original draft, Writing – review & editing. Frits Hilgen: Conceptualization, Methodology, Formal analysis, Writing – original draft, Writing – review & editing. Shinatria Adhityatama: Writing – review & editing. Klaudia Kuiper: Writing – original draft, Writing – review & editing. Josephine Joordens: Writing – review & editing, Funding acquisition.

Declaration of competing interest

The authors declare that they have no known competing financial interests or personal relationships that could have appeared to influence the work reported in this paper.

Data availability

This concerns a literature study, therefore all used data are publically available.

Acknowledgements

This study was carried out with the permission of the Indonesian National Research and Innovation Agency (BRIN research permits: 33/SIP/FRP/E5/Dit. KI/II/2018 and 12/E5/E5.4/SIP.EXT/2019 of Josephine Joordens; 8 B/TKPIPA/E5/Dit.KI/VIII/2018 and 2/TKPIPA/E%/Dit.KI/II/2019 of Sander Hilgen) under the project 'Studying Human Origin in East Java'. Special thanks to Dr. E. Pop for providing the map used in Fig. 1. We thank Linda Hinnov and Steve Meyers for discussing the MTM method and in particular the first order auto regression options and Josh Davies for discussing the Bchron approach and uncertainties in U–Pb LA-ICP-MS dating. Two anonymous reviewers are thanked for their comments, which led to a considerable improvement of the manuscript.

Appendix A. Supplementary data

Supplementary data related to this article can be found at https://doi.org/10.1016/j.quascirev.2022.107788.

References

Abdul Aziz, H., Hilgen, F.J., van Luijk, G.M., Sluijs, A., Kraus, M.J., Pares, J.M., Gingerich, P.D., 2008. Astronomical climate control on paleosol stacking patterns in the upper paleocene-lower eocene willwood formation, bighorn basin, Wyoming. Geology 36 (7), 531–534. https://doi.org/10.1130/G24734A.1.

Abels, H.A., Kraus, M.J., Gingerich, P.D., 2013. Precession-scale cyclicity in the fluvial lower eocene willwood formation of the bighorn basin, Wyoming (USA). Sedimentology 60 (6), 1467–1483. https://doi.org/10.1111/sed.12039.

Becker, J., Lourens, L.J., Hilgen, F.J., van der Laan, E., Kouwenhoven, T.J., Reichart, G.-J., 2005. Late Pliocene climate variability on Milankovitch to millennial time scales: a high-resolution study of MIS100 from the Mediterranean. Palaeogeogr. Palaeoclimatol. Palaeoecol. 228, 338–360. https://doi.org/10.1016/j.palaeo.2005.06.020.

Berghuis, H.W.K., Veldkamp, A., Adhityatama, S., Hilgen, S.L., Sutisna, I., Barianto, D.H., Pop, E.A., Reimann, T., Yurnaldi, D., Ekowati, D.R., 2021. Hominin homelands of East Java: revised stratigraphy and landscape reconstructions for plio-pleistocene trinil. Quat. Sci. Rev. 260, 1–27. https://doi.org/10.1016/j.quascirev.2021.106912.

Bettis, E.A., Milius, A.K., Carpenter, S.J., Larick, R., Zaim, Y., Rizal, Y., Ciochon, R., Tassier-Surine, S.A., Murray, D., Bronto, S., 2009. Way out of Africa: Early Pleistocene paleoenvironments inhabited by Homo erectus in Sangiran, Java. J. Hum. Evol. 56, 11–24.

Bettis III, E.A., Zaim, Y., Larick, R.R., Ciochon, R.L., Suminto, Rizal, Y., Reagan, M., Heizler, M., 2004. Landscape development preceding Homo erectus immigration into central Java, Indonesia: the Sangiran Formation lower lahar. Palaeogeogr. Palaeoclimatol. Palaeoecol. 206, 115–131. https://doi.org/10.1016/j.palaeo.2004.01.016.

Boës, X., Prat, S., Arrighi, V., Feibel, C., Haileab, B., Lewis, J., Harmand, S., 2019. Lake-level changes and hominin occupations in the arid Turkana basin during volcanic closure of the Omo River outflows to the Indian Ocean. Quat. Res. 91, 892–909. https://doi.org/10.1017/qua.2018.118.

Bond, G., Heinrich, H., Broecker, W., Labeyrie, L., Mcmanus, J., Andrews, J., Huon, S., Jantschik, R., Clasen, S., Simet, C., 1992. Evidence for massive discharges of icebergs into the North Atlantic ocean during the last glacial period. Nature 360 (6401), 245–249. https://doi.org/10.1038/360245a0.

Bosmans, J.H.C., Erb, M.P., Dolan, A.M., Drijfhout, S.S., Tuenter, E., Hilgen, F.J., Edge, D., Pope, J.O., Lourens, L.J., 2018. Response of the Asian summer monsoons to idealized precession and obliquity forcing in a set of GCMs. Quat. Sci. Rev. 188, 121–135. https://doi.org/10.1016/j.quascirev.2018.03.025.

Bosmans, J.H.C., Hilgen, F.J., Tuenter, E., Lourens, L.J., 2015. Obliquity forcing of low-latitude climate. Clim. Past 11, 1335–1346. https://doi.org/10.5194/cp-11-1335-2015.

Brasseur, B., 2009. Dynamique et histoire des dépôts du Pléistocène inférieur et moyen ancien dans le dôme de Sangiran (Java central, Indonésie). Ph.D. thesis. Département de Préhistoire. Muséum national d'Histoire naturelle.

Brasseur, B., Sémah, F., Sémah, A.-M., Djubiantono, T., 2015. Pedo-sedimentary dynamics of the Sangiran dome hominid bearing layers (Early to Middle Pleistocene, central Java, Indonesia): a palaeopedological approach for reconstructing 'Pithecanthropus' (Javanese Homo erectus) palaeoenvironment. Quat. Int. 376, 84–100. https://doi.org/10.1016/j.quaint.2014.05.030.

Channell, J.E.T., Singer, B.S., Jicha, B.R., 2020. Timing of Quaternary geomagnetic reversals and excursions in volcanic and sedimentary archives. Quat. Sci. Rev. 228, 1–28. https://doi.org/10.1016/j.quascirev.2019.106114.

deMenocal, P.B., 1995. Plio-pleistocene African climate. Science 270, 53–59. https://doi.org/10.1126/science.270.5233.53.

deMenocal, P.B., 2004. African climate change and faunal evolution during the Pliocene–Pleistocene. Earth Planet Sci. Lett. 220, 3–24. https://doi.org/10.1016/S0012-821X(04)00003-2.

deMenocal, P.B., Ortiz, J., Guilderson, T., Adkins, J., Sarnthein, M., Baker, L., Yarusinsky, M., 2000. Abrupt onset and termination of the African Humid Period: rapid climate responses to gradual insolation forcing. Quat. Sci. Rev. 19, 347–361. https://doi.org/10.1016/S0277-3791(99)00081-5.

DiNezio, P.N., Tierney, J.E., 2013. The effect of sea level on glacial Indo-Pacific climate. Nat. Geosci. 6, 485–491.

Drake, N.A., Blench, R.M., Armitage, S.J., Bristow, C.S., White, K.H., 2011. Ancient watercourses and biogeography of the sahara explain the peopling of the desert. Proc. Natl. Acad. Sci. U. S. A 108 (2), 458–462. https://doi.org/10.1073/pnas.1012231108.

Falguères, C., Sémah, F., Saleki, H., Hameau, S., Tu, H., Féraud, G., Simanjuntak, H., Widianto, H., 2016. Geochronology of early human settlements in Java: what is at stake? Quat. Int. 416, 5–11. https://doi.org/10.1016/j.quaint.2015.10.076.

Hajek, E.A., Straub, K.M., 2017. Autogenic sedimentation in clastic stratigraphy. Annu. Rev. Earth Planet Sci. 45, 681–709. https://doi.org/10.1146/annurev-earth-063016-015935.

Haslett, J., Parnell, A.C., 2008. A simple monotone process with application to radiocarbon-dated depth chronologies. J. Roy. Stat. Soc.: Series C (Applied Statistics) 57 (4), 399–418. https://doi/full/10.1111/j.1467-9876.2008.00623.x.

Head, M.J., Gibbard, P.L., 2005. Early-Middle Pleistocene transitions: an overview and recommendation for the defining boundary. Geol. Soc. Lond. Spec. Publ. 247, 1–18. https://doi.org/10.1144/GSL.SP.2005.247.01.01.

Heinrich, H., 1988. Origin and consequences of cyclic ice rafting in the northeast Atlantic Ocean during the past 130,000 years. Quat. Res. 29, 142–152. https://doi.org/10.1016/0033-5894(88)90057-9.

Hodell, David A., Channell, James E.T., Curtis, Jason H., Romero, Oscar E., Röhl, Ursula, 2008. Onset of "hudson strait" Heinrich events in the eastern north Atlantic at the end of the middle Pleistocene transition (~640 ka)? Paleoceanography 23 (4), PA4218. https://doi.org/10.1029/2008PA001591.

Hou, Z., Chen, S., Zhang, S., Yang, H., 2020. Sedimentary deformation features as evidence for paleoseismic events in the middle Eocene in the Dongying depression of the southern Bohai Bay basin, eastern China. Can. J. Earth Sci. 57 (8), 954–970. https://doi.org/10.1139/cjes-2019-0160.

Husson, L., Boucher, F.C., Sarr, A.-C., Sepulchre, P., Cahyarini, S.Y., 2020. Evidence of

Sundaland's subsidence requires revisiting its biogeography. J. Biogeogr. 47, 843–853. https://doi.org/10.1111/jbi.13762.
Huybers, P., 2009. Pleistocene glacial variability as a chaotic response to obliquity forcing. Clim. Past 5 (3), 481–488. https://doi.org/10.5194/cp-5-481-2009.
Hyodo, M., Matsu'ura, S., Kamishima, Y., Kondo, M., Takeshita, Y., Kitaba, I., Danhara, T., Aziz, F., Kurniawan, I., Kumai, H., 2011. High-resolution record of the Matuyama-Brunhes transition constrains the age of Javanese Homo erectus in the Sangiran dome, Indonesia. Proc. Natl. Acad. Sci. U. S. A 108, 19563–19568. https://doi.org/10.1073/pnas.1113106108.
Hyodo, M., Watanabe, N., Sunata, W., Susanto, E.E., Wahyono, H., 1993. Magneto-stratigraphy of hominid fossil bearing formations in Sangiran and Mojokerto, Java. Anthropol. Sci. 101, 157–186. https://doi.org/10.1537/ase.101.157.
Itihara, M., Sudijono, Kadar, D., Shibasaki, T., Kumai, H., Yoshikawa, S., Aziz, F., Soeradi, T., Wikarno, Kadar, A.P., Hasibuan, F., Kagemori, Y., 1985a. Geology and stratigraphy of the Sangiran area. In: Watanabe, N., Kadar, D. (Eds.), Quaternary Geology of the Hominid Fossil Bearing Formations in Java, pp. 11–43.
Itihara, M., Kadar, D., Watanabe, N., 1985b. Concluding remarks. In: Watanabe, N., Kadar, D. (Eds.), Quaternary Geology of the Hominid Fossil Bearing Formations in Java, pp. 367–378.
Itihara, M., Wikarno, Kagemori, Y., 1985c. Tektites from the Sangiran area. In: Watanabe, N., Kadar, D. (Eds.), Quaternary Geology of the Hominid Fossil Bearing Formations in Java, pp. 125–133.
Itihara, M., Watanabe, N., Kadar, D., Kumai, H., 1994. Quaternary stratigraphy of the hominid fossil bearing formations in the Sangiran area, Central Java. In: Franzen, J.L. (Ed.), 100 Years of Pithecanthropus; the *Homo Erectus* Problem, vol. 171. Courier Forschungs-Institut Senckenberg, pp. 123–128.
Joordens, J.C.A., Vonhof, H.B., Feibel, C.S., Lourens, L.J., Dupont-Nivet, G., van der Lubbe, J.H.J.L., Sier, M.J., Davies, G.R., Kroon, D., 2011. An astronomically-tuned climate framework for hominins in the Turkana Basin. Earth Planet Sci. Lett. 307, 1–8. https://doi.org/10.1016/j.epsl.2011.05.005.
Jourdan, F., Nomade, S., Wingate, M.T., Eroglu, E., Deino, A., 2019. Ultraprecise age and formation temperature of the Australasian tektites constrained by 40Ar/39Ar analyses. Meteorit. Planet. Sci. 54, 2573–2591. https://doi.org/10.1111/maps.13305.
Kaifu, Y., 2017. Archaic hominin populations in Asia before the arrival of modern humans: their phylogeny and implications for the "southern Denisovans. Curr. Anthropol. 58, 418–433. https://doi.org/10.1086/694318.
Kaifu, Y., Indriati, E., Aziz, F., Kurniawan, I., Baba, H., 2010. Cranial Morphology and variation of the earliest Indonesian hominids. In: Norton, C.J., Braun, D.R. (Eds.), Asian Paleoanthropology: from Africa to China and beyond, Vertebrate Paleobiology and Paleoanthropology. Springer Netherlands, Dordrecht, pp. 143–157. https://doi.org/10.1007/978-90-481-9094-2_11.
Khustina, Y.C., Solihin, D.D., Pratiwi, N.T., 2014. Morphological identification and Diversity analysis of fossil diatoms from diatomite Sangiran central Java Indonesia. J. Biol. Indones. 10.
Larick, R., Ciochon, R.L., Zaim, Y., Sudijono, Suminto, Rizal, Y., Aziz, F., Reagan, M., Heizler, M., 2001. Early Pleistocene 40Ar/39Ar ages for Bapang Formation hominins, central Jawa, Indonesia. Proc. Natl. Acad. Sci. USA 98, 4866–4871. https://doi.org/10.1073/pnas.081077298.
Leuschner, D.C., Sirocko, F., 2003. Orbital insolation forcing of the Indian Monsoon—a motor for global climate changes? Palaeogeogr. Palaeoclimatol. Palaeoecol. 197, 83–95. https://doi.org/10.1016/S0031-0182(03)00387-0.
Li, M., Hinnov, L., Kump, L., 2019. Acycle: time-series analysis software for paleoclimate research and education. Comput. Geosci. 127, 12–22. https://doi.org/10.1016/j.cageo.2019.02.011.
Lisiecki, L.E., Raymo, M.E., 2005. A Pliocene-Pleistocene stack of 57 globally distributed benthic δ18O records. Paleoceanography 20. https://doi.org/10.1029/2004PA001071.
Lourens, L.J., Becker, J., Bintanja, R., Hilgen, F.J., Tuenter, E., van de Wal, R.S.W., Ziegler, M., 2010. Linear and non-linear response of late Neogene glacial cycles to obliquity forcing and implications for the Milankovitch theory. Quat. Sci. Rev. 29 (1–2), 352–365. https://doi.org/10.1016/j.quascirev.2009.10.018.
Mann, M.E., Lees, J.M., 1996. Robust estimation of background noise and signal detection in climatic time series. Climatic Change 33, 409–445. https://doi.org/10.1007/BF00142586.
Mark, D.F., Renne, P.R., Dymock, R., Smith, V.C., Simon, J.I., Morgan, L.E., Staff, R.A., Ellis, B.S., 2017. High-precision $^{40}Ar/^{39}Ar$ dating of Pleistocene tuffs and temporal anchoring of the Matuyama-Brunhes boundary. Quat. Geochronol. 39, 1–23.
Matsu'ura, S., Kondo, M., Danhara, T., Sakata, S., Iwano, H., Hirata, T., Kurniawan, I., Setiyabudi, E., Takeshita, Y., Hyodo, M., Kitaba, I., Sudo, M., Danhara, Y., Aziz, F., 2020. Age control of the first appearance datum for Javanese *Homo erectus* in the Sangiran area. Science 367, 210–214. https://doi.org/10.1126/science.aau8556.
Meyers, S.R., 2014. Astrochron: an R Package for Astrochronology. https://cran.r-project.org/package=astrochron.
Mitchell, R.N., Bice, D.M., Montanari, A., Cleaveland, L.C., Christianson, K.T., Coccioni, R., Hinnov, L.A., 2008. Oceanic anoxic cycles? orbital prelude to the bonarelli level (OAE 2). Earth Planet Sci. Lett. 267 (1–2), 1–16. https://doi.org/10.1016/j.epsl.2007.11.026.
Morley, R.J., Morley, H.P., Zaim, Y., Huffman, O.F., 2020. Palaeoenvironmental setting of Mojokerto *Homo erectus*, the palynological expressions of Pleistocene marine deltas, open grasslands and volcanic mountains in East Java. J. Biogeogr. 47, 566–583. https://doi.org/10.1111/jbi.13770.
Naish, T., Abbott, S.T., Alloway, V., Beu, A.G., Carter, R.M., Edwards, A.R., Journeaux, T.D., Kamp, P.J., Pillans, B.J., Saul, G., 1998. Astronomical calibration of a southern hemisphere Plio-Pleistocene reference section, Wanganui Basin, New Zealand. Quat. Sci. Rev. 17, 695–710. https://doi.org/10.1016/S0277-3791(97)00075-9.
Naish, T., Kamp, P.J., 1997. Sequence stratigraphy of sixth-order (41 kyr) Pliocene–Pleistocene cyclothems, Wanganui basin, New Zealand: a case for the regressive systems tract. Geol. Soc. Am. Bull. 109, 978–999. https://doi.org/10.1130/0016-7606(1997)109<0978:SSOSOK>2.3.CO;2.
Ogg, J.G., 2020. Geomagnetic polarity time scale. In: Gradstein, F.M., Ogg, J.G., Schmitz, M.D., Ogg, G.M. (Eds.), Geologic Time Scale 2020. Elsevier, pp. 159–192.
Olsen, P.E., Kent, D.V., 1996. Milankovitch climate forcing in the tropics of Pangaea during the late Triassic. Palaeogeogr. Palaeoclimatol. Palaeoecol. 122, 1–26. https://doi.org/10.1016/0031-0182(95)00171-9.
Patterson, M., McKay, R., Naish, T., Escutia, C., Jiminezer-Espejo, F.J., Raymo, M.E., Meyers, S.R., Tauxe, L., Brinkhuis, H., 2014. Orbital forcing of the east Antarctic ice sheet during the pliocene and early Pleistocene. Nat. Geosci. 7, 841–847. https://doi.org/10.1038/ngeo2273.
Potts, R., Faith, J.T., 2015. Alternating high and low climate variability: the context of natural selection and speciation in Plio-Pleistocene hominin evolution. J. Hum. Evol., Environmental Variability and Hominin Dispersal 87, 5–20. https://doi.org/10.1016/j.jhevol.2015.06.014.
R Core Team, 2022. R: A Language and Environment for Statistical Computing. R Foundation for Statistical Computing, Vienna, Austria.
Reichart, G.-J., 1997. Late Quaternary Variability of the Arabian Sea Monsoon and Oxygen Minimum Zone (PhD Thesis). Utrecht University.
Rizal, Y., Westaway, K.E., Zaim, Y., van den Bergh, G.D., Bettis, E.A., Morwood, M.J., Huffman, O.F., Grün, R., Joannes-Boyau, R., Bailey, R.M., Sidarto, Westaway, M.C., Kurniawan, I., Moore, M.W., Storey, M., Aziz, F., Suminto, Zhao, J., Aswan, Sipola, M.E., Larick, R., Zonneveld, J.-P., Scott, R., Putt, S., Ciochon, R.L., 2020. Last appearance of Homo erectus at f, Java, 117,000–108,000 years ago. Nature 577, 381–385. https://doi.org/10.1038/s41586-019-1863-2.
Saleki, H., Féraud, G., Sémah, F., Falguères, C., Sémah, A.M., Djubiantono, T., 1998. Datations radiométriques des couches à Homo erectus de Kabuh à Ngebung (Sangiran, Java central, Indonésie). Actes XIIIe Congrès UISPP Forli Ital. 2, 63–74.
Sarr, A.-C., Sepulchre, P., Husson, L., 2019a. Impact of the Sunda shelf on the climate of the Maritime continent. J. Geophys. Res. Atmospheres 124, 2574–2588. https://doi.org/10.1029/2018JD029971.
Sarr, A.-C., Husson, L., Sepulchre, P., Pastier, A.-M., Pedoja, K., Elliot, M., Arias-Ruiz, C., Solihuddin, T., Aribowo, S., Susilohadi, 2019b. Subsiding Sundaland. Geology 47 (2), 119–122. https://doi.org/10.1130/G45629.1.
Sémah, A.-M., 1982. A preliminary report on a Sangiran pollen diagram. Prelim. Rep. SANGIRAN POLLEN Diagr.
Sémah, A.-M., Sémah, F., Djubiantono, T., Brasseur, B., 2010. Landscapes and hominids' environments: changes between the lower and the early middle Pleistocene in Java (Indonesia). Quat. Int. 223, 451. https://doi.org/10.1016/j.quaint.2009.07.017.
Sémah, F., 1982. Pliocene and Pleistocene geomagnetic reversals recorded in the geomolong and Sangiran domes (central Java). Mod. Quaternary Res. SE Asia 7, 151–164.
Sémah, F., Saleki, H., Falguères, C., Féraud, G., Djubiantono, T., 2000. Did early man reach Java during the late pliocene? J. Archaeol. Sci. 27, 763–769. https://doi.org/10.1006/jasc.1999.0482.
Sémah, F., Sémah, A.-M., 1985. Environnement des premiers mammifères et hominidés de Java in Séance du 23-X-85 : archéologie française à l'étranger. Bull. Société Préhistorique Fr. Comptes Rendus Séances Mens. Paris 82.
Shimizu, Y., Mubroto, B., Siagian, H., Untung, M., 1985. A paleomagnetic study in the Sangiran area. In: Watanabe, N., Kadar, D. (Eds.), Quaternary Geology of the Hominid Fossil Bearing Formations in Java, pp. 275–307.
Sondaar, P., 1996. Faunal change and hominid evolution during Quaternary Java. Geol. Res. Dev. Cent. Paleontol. Ser. 8, 1–10.
Storm, P., 2001. The evolution of humans in Australasia from an environmental perspective. Palaeogeogr. Palaeoclimatol. Palaeoecol., Quaternary Environmental Change in the Indonesian Region 171, 363–383. https://doi.org/10.1016/S0031-0182(01)00254-1.
Suzuki, M., Wikarno, Budisantoso, Saefudin, I., Itihara, M., 1985. Fission track ages of pumice tuff, tuff layers and Javites of hominid fossil bearing formations in Sangiran area, Central Java. In: Watanabe, N., Kadar, D. (Eds.), Quaternary Geology of the Hominid Fossil Bearing Formations in Java, pp. 309–357.
Thomson, D.J., 1982. Spectrum estimation and harmonic analysis. Proc. IEEE 70, 1055–1096. https://doi.org/10.1109/PROC.1982.12433.
Tiedemann, R., Sarnthein, M., Shackleton, N.J., 1994. Astronomic timescale for the pliocene Atlantic δ18O and dust flux records of ocean Drilling program site 659. Paleoceanography 9, 619–638. https://doi.org/10.1029/94PA00208.
Timmermann, A., Friedrich, T., 2016. Late Pleistocene climate drivers of early human migration. Nature 538, 92–95. https://doi.org/10.1038/nature19365.
Tokunaga, S., Oshima, H., Polhaupessy, A.A., Ito, Y., 1985. A palynological study of the Pucangan and Kabuh formations in the Sangiran area. In: Watanabe, N., Kadar, D. (Eds.), Quaternary Geology of the Hominid Fossil Bearing Formations in Java, pp. 199–218.
Trauth, M.H., Asrat, A., Berner, N., Bibi, F., Foerster, V., Grove, M., Kaboth-Bahr, S., Maslin, M.A., Mudelsee, M., Schäbitz, F., 2021. Northern hemisphere glaciation, African climate and human evolution. Quat. Sci. Rev. 268, 107095. https://doi.org/10.1016/j.quascirev.2021.107095.
Trauth, M.H., Maslin, M.A., Deino, A.L., Strecker, M.R., Bergner, A.G.N., Dühnforth, M., 2007. High- and low-latitude forcing of Plio-Pleistocene East African climate

and human evolution. J. Hum. Evol., African Paleoclim. Human Evol. 53, 475–486. https://doi.org/10.1016/j.jhevol.2006.12.009.
van den Bergh, G.D., de Vos, J., Sondaar, P.Y., 2001. The Late Quaternary palaeogeography of mammal evolution in the Indonesian Archipelago. Palaeogeogr. Palaeoclimatol. Palaeoecol., Quaternary Environmental Change in the Indonesian Region 171, 385–408. https://doi.org/10.1016/S0031-0182(01)00255-3.
van Gorsel, J.T., Troelstra, S.R., 1981. Late Neogene planktonic foraminiferal biostratigraphy and climatostratigraphy of the Solo River section (Java, Indonesia). Mar. Micropaleontol. 6, 183–209. https://doi.org/10.1016/0377-8398(81)90005-0.
Volmer, R., van der Geer, A., Cabrera, P.A., Wibowo, P.W., Kurniawan, I., 2019. When did Cuon reach Java? – reinvestigation of canid fossils from Homo erectus faunas. Geobios 55, 89–102. https://doi.org/10.1016/j.geobios.2019.06.004.
Vrba, E.S., 1988. Late Pliocene climatic events and hominid evolution. Evol. Hist. "robust" Australopithecines 405–426.
Quaternary geology of the hominid fossil bearing formations in Java. In: Watanabe, N., Kadar, D. (Eds.), Geol. Res. Dev. Cent. Spec. Publ. 4, 1–378.